

Review

Not peer-reviewed version

Wide and Ultrawide Bandgap Power Semiconductors: A Comprehensive System-Level Review

[Giuseppe Galioto](#), [Gianpaolo Vitale](#)^{*}, [Antonino Sferlazza](#), [Giuseppe Lullo](#), [Giuseppe Costantino Giaconia](#)

Posted Date: 5 February 2026

doi: 10.20944/preprints202601.2280.v2

Keywords: efficiency; gallium nitride (GaN); power density; silicon carbide (SiC); wide-bandgap (WBG); ultrawide-bandgap (UWBG); power electronics; electric vehicles; EMI mitigation; vertical GaN; bidirectional switch (BDS); systematic review; PRISMA methodology



Preprints.org is a free multidisciplinary platform providing preprint service that is dedicated to making early versions of research outputs permanently available and citable. Preprints posted at Preprints.org appear in Web of Science, Crossref, Google Scholar, Scilit, Europe PMC.

Copyright: This open access article is published under a [Creative Commons CC BY 4.0 license](#), which permit the free download, distribution, and reuse, provided that the author and preprint are cited in any reuse.

Disclaimer/Publisher's Note: The statements, opinions, and data contained in all publications are solely those of the individual author(s) and contributor(s) and not of MDPI and/or the editor(s). MDPI and/or the editor(s) disclaim responsibility for any injury to people or property resulting from any ideas, methods, instructions, or products referred to in the content.

Systematic Review

Wide and Ultrawide Bandgap Power Semiconductors: A Comprehensive System-Level Review

Giuseppe Galieto¹ , Gianpaolo Vitale^{2*} , Antonino Sferlazza¹ , Giuseppe Lullo¹  and Giuseppe Costantino Giaconia¹ 

¹ Department of Engineering, University of Palermo, Viale delle Scienze, Building 9, 90128 Palermo, Italy

² Institute for High Performance Computing and Networking (ICAR), National Research Council of Italy, Via Ugo La Malfa 153, 90146 Palermo, Italy

* Correspondence: gianpaolo.vitale@icar.cnr.it

Abstract

This review analyzes the transition from silicon to wide-bandgap (WBG) and ultrawide-bandgap (UWBG) semiconductor materials for power electronics, focusing on Silicon Carbide (SiC) and Gallium Nitride (GaN) technologies. Following a PRISMA-based systematic review methodology, we analyzed more than 50 peer-reviewed publications spanning device technology, converter architectures, and system applications. We employ a bottom-up approach, progressing from fundamental material properties through device architectures and converter topologies to system-level implications. We examine how intrinsic material properties enable operation at elevated temperatures, voltages, and frequencies while minimizing losses. Through analysis of Figures of Merit and system-level Key Performance Indicators, we quantify WBG benefits across automotive, industrial, renewable energy, and consumer electronics sectors, demonstrating 3–5x power density improvements and 20–40% cost reductions. The review presents emerging device technologies including vertical GaN for medium-voltage applications and monolithic bidirectional switches (BDS) enabling single-stage power conversion. We provide the first comprehensive topology-level comparison of emerging vertical GaN and monolithic bidirectional switches against established SiC solutions, identifying specific applications where each technology offers advantages. A comprehensive topology-by-topology comparison between SiC and GaN is provided, offering design guidelines for device selection. The review addresses practical constraints including dynamic on-resistance degradation, threshold voltage instability, and electromagnetic interference challenges for both SiC and GaN. Finally, we examine emerging UWBG materials (β -Ga₂O₃, AlN, c-BN, Diamond) and their development status, manufacturing challenges, supply chain considerations, and commercialization prospects for ultra-high-voltage applications.

Keywords: efficiency; gallium nitride (GaN); power density; silicon carbide (SiC); wide-bandgap (WBG); ultrawide-bandgap (UWBG); power electronics; electric vehicles; EMI mitigation; vertical GaN; bidirectional switch (BDS); systematic review; PRISMA methodology

1. Introduction

The global power electronics sector is experiencing a transformative shift driven by increasingly stringent demands for sustainable energy systems, improved operational efficiency, and reduced carbon emissions. In 2024, energy-related carbon dioxide (CO₂) emissions reached approximately 36.3 Gt, representing an increase of roughly 0.9% compared to 2023 [1]. Although the adoption of clean energy technologies—including solar photovoltaics, wind power, and electric vehicles—has tempered the rate of emissions growth, these persistently high emission levels underscore that incremental improvements alone are insufficient; substantial efficiency gains across the entire energy conversion chain are essential [2].

The historical trend of global carbon dioxide emissions from energy and industrial sources (1970–2024), highlighting the urgency of reducing emissions growth through more efficient power conversion

technologies is shown in Figure 1. Based on these charts, global CO₂ emissions have more than doubled from 15.0 GtCO₂/year in 1970 to 36.3 GtCO₂/year in 2024, showing a steady upward trend over five decades. The only notable interruption was a temporary decrease down to 33.3 GtCO₂/year in 2020, likely due to pandemic-related economic slowdowns, followed by a rapid rebound in subsequent years.

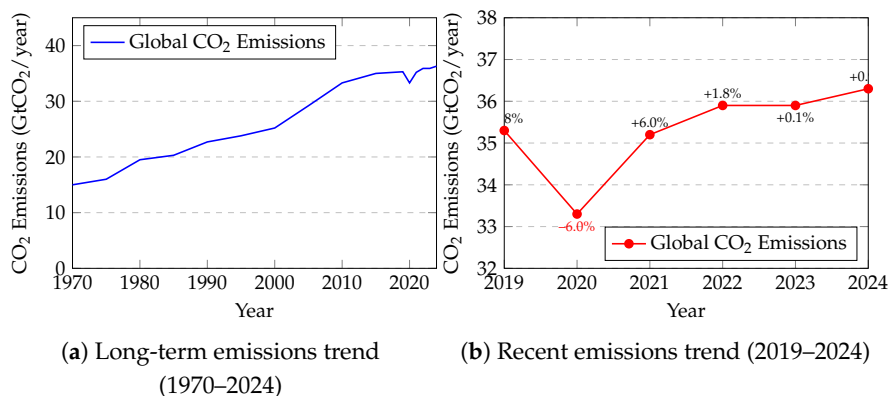


Figure 1. Global energy-related and industrial CO₂ emissions (1970–2024). (a) CO₂ Emissions over the last 54 years, (b) CO₂ Emissions in last 5 years showing year-over-year percentage changes. Data arranged from: Deng et al. [2].

Central to addressing this challenge is the transition from traditional silicon-based power semiconductors to wide-bandgap (WBG) and ultrawide-bandgap (UWBG) materials, most notably Silicon Carbide (SiC) and Gallium Nitride (GaN) [3,4]. This technological evolution represents far more than a simple material substitution; it constitutes a paradigm shift in power conversion capability that enables revolutionary improvements in efficiency, power density, and thermal performance across virtually all application domains [5–7].

The cascading benefits of improved power electronics efficiency across different application sectors demonstrate how WBG technology contributes to overall system sustainability through environmental, economic, and technical improvements. These factors are summed up in Figure 2, where a 2-5% efficiency improvement in WBG devices translates into reduced carbon footprints and lower energy waste environmentally, reduced electricity costs and lower cooling requirements economically, and higher power density with increased switching frequency technically.

Efficiency Improvements and System Benefits

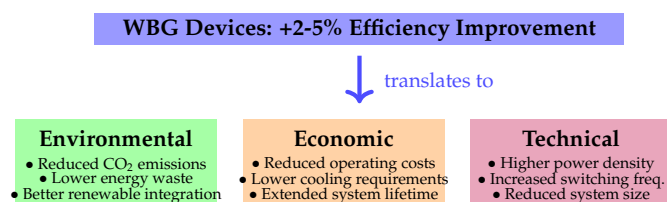


Figure 2. Key benefits of WBG technology across different application sectors

Power converters based on semiconductor switching devices regulate energy flow in nearly every modern electrical system, from renewable energy installations and electric vehicle drivetrains to industrial motor drives and data center infrastructure. Even modest improvements in converter efficiency—on the order of 2–5%—can yield substantial reductions in overall energy consumption and associated emissions when deployed at scale [8,9]. The cascading benefits of WBG technology extend beyond raw efficiency improvements to encompass reduced cooling requirements, smaller passive components, and enhanced system reliability.

The economic case for WBG adoption is equally compelling. In large-scale facilities such as data centers operating 10 MW of server power supplies, improving efficiency from 94% to 98% through

advanced GaN and SiC power supply units can result in annual energy savings exceeding \$700k while simultaneously reducing cooling requirements by nearly halving power delivery network losses from 17% to approximately 9% [10]. For electric vehicles, a 5–10% efficiency improvement from SiC-based 800V traction inverters translates to approximately 7% additional driving range without increasing battery capacity, directly enhancing user experience while reducing battery degradation and total cost of ownership [11,12].

This review paper provides a comprehensive analysis of the current state and future prospects of WBG and UWBG power semiconductors using a bottom-up approach. Section 2 presents fundamental material properties and comparative analysis through various figures of merit. Section 3 provides an in-depth analysis of emerging UWBG materials including their development status and commercialization timeline. Section 4 analyzes SiC and GaN device configurations. Section 5 addresses converter topologies for both SiC and GaN devices. Section 6 provides a comprehensive SiC vs. GaN comparison including gate driver requirements. Section 7 presents system-level dynamic validation through Double Pulse Test simulations comparing GaN and SiC switching behavior. Section 8 discusses system-level implications and quantifies benefits across multiple performance dimensions. Section 9 examines the application landscape with detailed case studies. Section 10 covers reliability considerations and practical constraints for both SiC and GaN technologies. Finally, Section 11 provides conclusions and future research directions. The list of acronyms is provided at the end of the document.

1.1. Literature Review Methodology

This review follows a systematic approach adapted from the PRISMA (Preferred Reporting Items for Systematic Reviews and Meta-Analyses) guidelines to ensure transparency, reproducibility, and comprehensiveness in the literature selection process [13].

1.1.1. Search Strategy and Databases

The literature search was conducted across multiple academic databases including IEEE Xplore, ScienceDirect, Web of Science, Scopus, and Google Scholar. The search period covered publications from January 2014 to December 2025, capturing the critical decade of WBG commercialization and maturation. The primary search keywords and Boolean combinations employed were:

- Primary keywords: “wide bandgap semiconductors”, “silicon carbide power devices”, “gallium nitride HEMT”, “SiC MOSFET”, “GaN power electronics”
- Secondary keywords: “ultrawide bandgap”, “power converter topology”, “electric vehicle inverter”, “DC-DC converter”, “gate driver design”
- Emerging technology keywords: “vertical GaN”, “bidirectional switch”, “gallium oxide power”, “diamond semiconductor”, “aluminum nitride”
- Application keywords: “traction inverter”, “on-board charger”, “solar inverter”, “data center power supply”

Boolean combinations such as (“SiC” OR “GaN”) AND (“power converter” OR “inverter” OR “DC-DC”) AND (“efficiency” OR “power density” OR “switching frequency”) were employed to capture the intersection of device technology and converter applications.

1.1.2. Screening and Selection Process

Figure 3 presents the PRISMA flow diagram illustrating the systematic literature selection process.

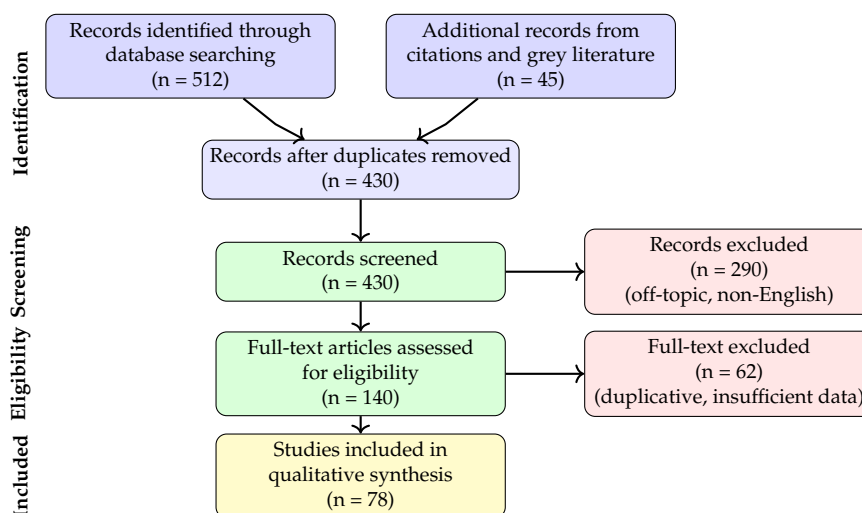


Figure 3. PRISMA flow diagram for systematic literature selection process.

Table 1 summarizes the distribution of selected literature by category.

Table 1. Distribution of Reviewed Literature by Category

Category	Papers Reviewed	Key Focus Areas
SiC Device Technology	12	MOSFET structures, trench devices, reliability, failure modes
GaN HEMT Technology	13	E-mode/D-mode, dynamic R_{on} , trapping effects
Converter Topologies	10	DAB, Buck, Inverters, Magnetics, Wireless Power
System Applications	14	EV Traction, Hydrogen, Data Centers, Solar
UWBG Materials	12	Ga_2O_3 , AlN, Diamond, c-BN, Heterostructures
EMI, Thermal & Pkg	11	Gate drivers, layout, thermal management, packaging
Emerging Technologies	3	Vertical GaN, Fin-JFETs
Fundamentals & Surveys	3	Figures of Merit, Methodology, Historical Trends
Total	78	—

1.1.3. Inclusion and Exclusion Criteria

Studies were included if they: (1) presented original research or comprehensive reviews on WBG/UWBG power semiconductor devices; (2) provided quantitative data on device performance, converter efficiency, or system-level benefits; (3) were published in peer-reviewed journals or major IEEE conference proceedings; (4) addressed practical implementation aspects including reliability, EMI, or thermal management.

Studies were excluded if they: (1) focused exclusively on RF/microwave applications without power electronics relevance; (2) presented only simulation results without experimental validation; (3) were superseded by more comprehensive studies from the same research group; (4) lacked quantitative performance metrics for comparison.

1.2. Comparison with Existing Review Literature and Added Value

Table 2 presents a systematic comparison between this review and recent similar publications, highlighting the unique contributions and gaps addressed by this work. While existing reviews focus on specific aspects such as industrial device reliability, material properties, thermal management,

or sustainability perspectives, this 2026 review uniquely provides a comprehensive system-level analysis of both WBG and UWBG technologies. Our work addresses the limitations of prior works by incorporating emerging device coverage (vertical GaN and monolithic BDS), detailed converter topology comparisons, quantitative economic analysis, and up-to-date commercial landscapes through 2025.

Table 2. Comparison with Recent WBG Semiconductor Review Papers.

Year	Scope	Strengths	Limitations
2024	Industrial SiC/GaN devices	Excellent reliability analysis; commercial device survey; trapping mechanisms	Limited topology comparison; no UWBG coverage; no economic analysis
2023	WBG/UWBG overview	Broad material coverage; historical context; FOM analysis	Limited system-level analysis; no vertical GaN/BDS; no design guidelines
2025	Carbon neutrality focus	Sustainability perspective; policy implications; grid integration	Limited converter topology detail; no practical design constraints
2022	Material properties	Comprehensive FOM analysis; device physics	Dated commercial landscape (2022); no emerging devices; limited applications
2017	SiC power devices	Deep SiC device analysis; HVDC applications; converter topologies	Pre-dates GaN maturation; no UWBG coverage; limited GaN comparison
2023	GaN power devices	Comprehensive GaN focus; DC-DC and DC-AC applications	SiC comparison limited; no UWBG materials; no system-level KPIs
2026	System-level WBG/UWBG	See Added Value below	—

Beyond the comprehensive reviews compared in Table 2, several specialized reviews provide valuable insights into specific technical domains. In thermal management, Belguith et al. [19] present advanced cooling techniques for high-power-density GaN converters, while Qin et al. [20] and Zhou et al. [21] address device-level thermal management and packaging challenges for WBG and UWBG devices. For electromagnetic compatibility, Zhang and Wang [22] provide a comprehensive EMI survey addressing the challenges introduced by fast WBG switching transients. In the UWBG domain, Donato et al. [23] present the state of the art for diamond power devices, while Green et al. [24] examine β -Ga₂O₃ power electronics specifically. For reliability, Akbar et al. [25] focus on SiC MOSFET failure modes, complementing the broader reliability coverage in this review. Additionally, Adeloje et al. [26] provide a recent comparative review of GaN in electric vehicle systems. The work by Wu et al. [27] was considered as not concurrent in this review and it was included as a reference in Section 6.5.2.

1.2.1. Unique Contributions and Added Value

This review addresses several critical gaps in the existing literature:

(1) Comprehensive Topology-by-Topology SiC vs. GaN Comparison: Unlike previous reviews that focus primarily on device-level characteristics, this work provides detailed design guidelines for device selection across all major converter topologies (Table 12), enabling practicing engineers to make informed technology choices based on specific application requirements. While She et al. [17] and Musumeci & Barba [18] address converter applications, neither provides systematic topology-level selection criteria spanning both SiC and GaN with quantitative metrics.

(2) Emerging Device Technologies: This review provides the first comprehensive coverage of vertical GaN power devices and monolithic bidirectional switches (BDS) in the context of converter topologies. While Buffolo et al. [8] acknowledge these technologies, our work provides detailed analysis of their impact on specific topologies including matrix converters, Vienna rectifiers, and current-source inverters—analysis absent from all prior reviews.

(3) **Updated UWBG Materials Assessment:** The UWBG section (Section 3) incorporates the latest developments through 2025. Previous reviews [3,16] lack these recent milestones, and even the 2023 UWBG coverage in Rafin et al. [14] does not capture these 2024–2025 advances.

(4) **Bottom-Up Systematic Approach:** This review uniquely employs a bottom-up methodology (Materials → Devices → Converters → Systems), providing clear traceability from fundamental material properties through figures of merit to system-level KPIs. This approach enables readers to understand *why* specific devices excel in particular applications—a framework absent from prior works that typically separate device physics from application discussions.

(5) **Quantitative System-Level Benefits:** Section 8 provides quantified economic analysis with payback periods for each application sector (Table 14)—data largely absent from device-focused reviews. While Chow et al. [15] discuss system-level sustainability, they do not provide the sector-specific economic quantification presented here.

(6) **Practical Design Constraints:** The review addresses real-world implementation challenges including dynamic R_{on} degradation mechanisms, threshold voltage instability, and gate driver optimization requirements (Table 11) that are often overlooked in material-focused surveys. Although Akbar et al. [25] address SiC reliability and Musumeci & Barba [18] discuss GaN challenges, neither integrates these constraints with topology-specific design guidelines as presented here.

Table 3 demonstrates that this review uniquely bridges the gap between device-centric technical analyses and application-level discussions through three key dimensions. The *New Data* contributions (vGaN/BDS coverage, 2025 UWBG updates) address the temporal lag in existing reviews, while the *New Framework* (bottom-up methodology, PRISMA compliance) provides transparent systematic analysis absent in prior work. Most critically, the *New Insights* deliver actionable quantitative guidance—topology-specific device selection criteria and economic payback analysis—that enable engineers to translate theoretical WBG advantages into practical deployment decisions across automotive, industrial, and renewable energy applications.

Table 3. Key Novelty Summary: Unique Contributions Relative to Comparative Literature

Dimension	New Data	New Insights	New Framework
Comparative (2)	9 topologies compared: VSI, Buck, DAB, Vienna, T-type/NPC, LLC, Matrix, HERIC, CSI	First systematic SiC/GaN/vGaN/BDS device selection criteria with quantitative metrics	Decision guidelines based on voltage class, power level, and switching frequency
Devices	vGaN: 1.2 kV/50 A with 50% loss reduction vs. lateral GaN; BDS: 650–850 V monolithic four-quadrant operation	First converter-level vGaN/BDS impact analysis on 8 topologies (Table 8); commercialization timeline 2025–2030	Technology selection: vGaN for 650 V–1.2 kV unidirectional; BDS for bidirectional/single-stage conversion
Materials	β -Ga ₂ O ₃ : 4" wafers, 2.3 kV; AlN: 7.3 MV/cm; Diamond: 4.6 kV SBD; c-BN: 6.4 eV bandgap	TRL assessment (2–6); projected commercialization: β -Ga ₂ O ₃ 2027–30, AlN/Diamond 2030–35, c-BN \geq 2035	Material-to-application mapping: β -Ga ₂ O ₃ for 600 V–3.3 kV, AlN for 10 kV+/RF, Diamond for extreme power
Framework	6 Figure of Merits analyzed: BFOM, BHFFOM, JFOM, KFOM, CHFFOM, TFOM (Table 5)	Clear traceability from material properties (E_g , E_c , μ_n , κ) through device FOMs to system-level KPIs	4-tier methodology: Materials → Devices → Converters → Systems; PRISMA-compliant review
Analysis	6 sectors: Data center (\$450k/yr), EV (+20 km), Solar PV (\$35k/yr), Industrial VFD (\$22k/yr), Telecom (\$8k/site), Aerospace (–15 kg)	Payback periods: 1.5 yr (data center), 2 yr (solar), 2.5 yr (industrial); immediate ROI for EV range and aerospace weight	Sector-specific efficiency gains: 94→97% (data center), 96→99% (EV traction), 92→95% (telecom)
Constraints	Dynamic R_{on} : 2–5× degradation; V_{th} instability; short-circuit withstand: GaN <1 μ s, SiC 2–5 μ s	8 mitigation strategies: negative gate bias, active Miller clamping, desaturation detection (<200 ns), optimized buffer designs	Gate driver requirements matrix (Table 11): V_{GS} , Q_g , propagation delay, CMTI

1.2.2. Research Gap Analysis

Figure 4 illustrates the positioning of this review relative to existing literature across two key dimensions: device technology depth and system integration scope. This review uniquely spans from fundamental device technology through system-level integration while incorporating emerging UWBG technologies, distinguishing itself from prior works that either focused narrowly on device/material aspects [8,16,23] or emphasized system-level applications without comprehensive device coverage [14, 15].

The landscape of WBG review literature reveals three distinct clusters: (i) device-focused reviews that provide deep technical analysis but limited application guidance [8,16,25]; (ii) material-focused reviews covering emerging UWBG semiconductors but lacking converter-level analysis [3,23,24]; and (iii) application-focused reviews addressing specific sectors but without systematic device comparison [18,26]. This review bridges these clusters through its bottom-up methodology and comprehensive scope.

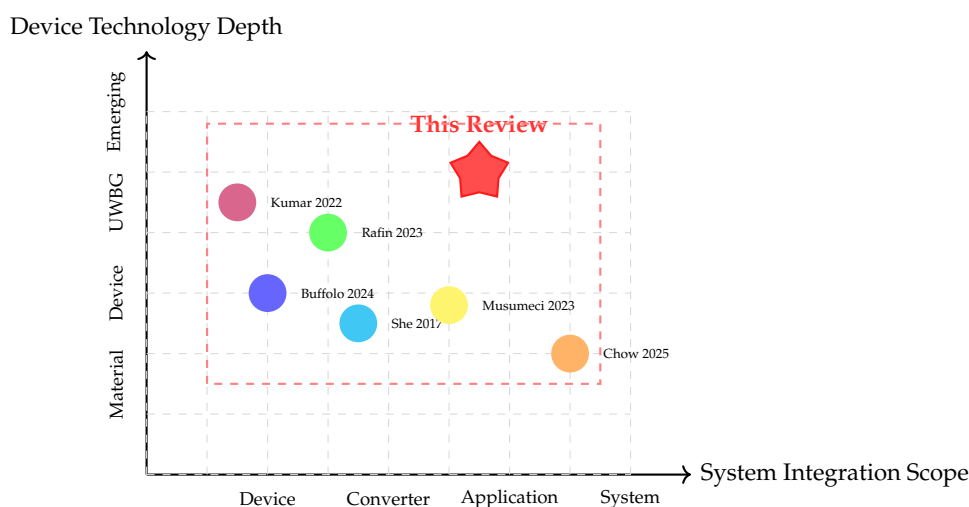


Figure 4. Positioning of this review relative to existing WBG literature. This work uniquely spans from fundamental device technology through system-level integration while incorporating emerging technologies (vertical GaN, BDS, UWBG materials). The dashed rectangle indicates the comprehensive coverage achieved by our bottom-up systematic approach.

2. Material Properties and Comparative Analysis

The fundamental material properties of semiconductors determine the ultimate performance limits achievable in power electronic devices. WBG and UWBG materials demonstrate exceptional versatility across power electronics and Radio Frequency (RF) applications due to their capacity to operate reliably in high-temperature and harsh environments [4,16].

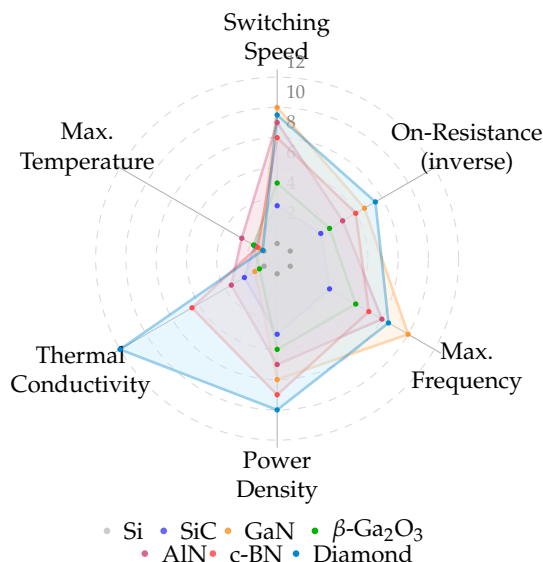
2.1. Intrinsic Material Characteristics

Table 4 summarizes the key properties of silicon alongside WBG materials (4H-SiC, GaN) and emerging UWBG materials (β -Ga₂O₃, AlN, c-BN, Diamond). The UWBG materials exhibit significantly superior properties compared to silicon, with bandgaps ranging from 4.9 to 6.4 eV and breakdown fields of 8–15 MV/cm, though trade-offs exist in electron mobility and thermal conductivity, where diamond leads with 23 W/cm·K and GaN achieves the highest mobility at 2000 cm²/Vs.

Table 4. Material Properties of Semiconductors for Power Electronics, data taken from [3].

Parameter	Si	4H-SiC	GaN	β -Ga ₂ O ₃	AlN	c-BN	Diamond
E_g (eV)	1.12	3.23	3.4	4.9	6.2	6.4	5.5
E_c (MV/cm)	0.3	2.5	3.3	8	15	12	10
μ_n (cm ² /Vs)	1440	950	2000	250	850	200	4500
v_{sat} (10 ⁷ cm/s)	1.0	2.0	2.4	1.1	1.4	2.0	2.3
κ (W/cm·K)	1.5	3.7	2.5	0.1–0.3	2.85	13	23

Figure 5 provides a comprehensive radar chart comparison between silicon and U/WBG devices across multiple key parameters, visually demonstrating the performance advantages of advanced semiconductor materials. Diamond and c-BN exhibit exceptional thermal conductivity and maximum temperature capabilities, while GaN achieves superior switching speed and maximum frequency, and SiC offers a balanced profile with strong performance across on-resistance, power density, and thermal management, clearly outperforming silicon in all metrics.

**Figure 5.** Radar chart comparison of power semiconductor materials. Normalized performance relative to Si (adapted from [3,4]).

The bandgap energy E_g represents the energy required to excite an electron from the valence band to the conduction band. Materials with larger bandgaps exhibit higher intrinsic breakdown voltages and can operate at elevated temperatures without excessive thermally-generated leakage current [5]. The wide bandgap of SiC (3.23 eV) and GaN (3.4 eV) compared to silicon (1.12 eV) fundamentally enables operation at higher voltages and temperatures.

The critical electric field E_c defines the maximum electric field a material can sustain before avalanche breakdown occurs [17]. SiC and GaN exhibit critical fields approximately 8–11 \times higher than silicon, while UWBG materials such as β -Ga₂O₃ and AlN approach 30–50 \times improvement.

Electron mobility μ_n quantifies how rapidly charge carriers drift through the material under an applied electric field [28]. While SiC exhibits somewhat lower mobility than silicon (950 vs. 1440 cm²/Vs), GaN offers superior mobility (2000 cm²/Vs), and diamond presents exceptional mobility (4500 cm²/Vs) for future applications.

Thermal conductivity κ governs the ability to conduct heat away from active device regions, critically impacting power handling capability and long-term reliability [29]. SiC's thermal conductivity

(3.7 W/cm · K) substantially exceeds that of silicon (1.5 W/cm · K), while diamond's exceptional value (23 W/cm · K) positions it as the ultimate material for extreme power density applications.

2.2. Quantitative Performance Metrics: Figures of Merit

Several Figures of Merit (FOMs) have been developed to enable quantitative comparison of semiconductor technologies [30–33].

Baliga's Figure of Merit (BFOM) characterizes the trade-off between on-resistance and breakdown voltage for unipolar power devices [30]:

$$\text{BFOM} = \frac{\epsilon_r \mu_n E_c^3}{4} \quad (1)$$

Baliga High-Frequency Figure of Merit (BHFFOM) accounts for switching losses [34]:

$$\text{BHFFOM} = \frac{\mu_n E_c^2}{2\pi} \quad (2)$$

Johnson's Figure of Merit (JFOM) characterizes the maximum power-frequency product [31]:

$$\text{JFOM} = \left(\frac{v_{sat} E_c}{2\pi} \right)^2 \quad (3)$$

Keyes' Figure of Merit (KFOM) evaluates thermal management and power density limits [32]:

$$\text{KFOM} = \frac{\kappa \cdot v_{sat}}{4\pi\epsilon_0\epsilon_r} \quad (4)$$

Combined High-Frequency Figure of Merit (CHFFOM) extends BHFFOM to include thermal effects [33]:

$$\text{CHFFOM} = \kappa \cdot \text{BHFFOM} = \frac{\kappa \mu_n E_c^2}{2\pi} \quad (5)$$

Thermal Figure of Merit (TFOM) [19] specifically addresses heat dissipation capability:

$$\text{TFOM} = \frac{\lambda}{k_B T} \quad (6)$$

where k_B is Boltzmann's constant and T is absolute temperature.

Table 5 presents normalized FOM values relative to silicon. Diamond demonstrates the highest performance across all FOMs with BFOM of 50000× and CHFFOM of 2114× relative to silicon, while β -Ga₂O₃ excels in BFOM (3444×) but shows lower performance in frequency-related metrics, and GaN offers a balanced profile with strong BFOM (846×) and competitive performance across switching and thermal FOMs.

Table 5. Normalized Figures of Merit for Power Semiconductor Materials (Si = 1) data taken from [3,30,33].

Material	BFOM	BHFFOM	JFOM	KFOM	CHFFOM	TFOM
Si	1	1	1	1	1	1
4H-SiC	317	13.7	20	4.8	29	3.3
GaN	846	27.5	33	1.4	56	2.2
β -Ga ₂ O ₃	3444	10.5	14	0.9	30	0.8
AlN	3360	57.6	68	13.8	562	9.2
Diamond	50000	81.2	163	46.2	2114	33

3. Emerging UWBG Materials: Development Status and Commercialization

While SiC and GaN technologies have achieved commercial maturity, ultrawide-bandgap (UWBG) materials represent the next frontier in power semiconductor development. These materials, char-

acterized by bandgaps exceeding 4 eV, offer theoretical performance advantages that could enable applications beyond the capabilities of current WBG devices [3].

3.1. Beta-Gallium Oxide (β -Ga₂O₃)

β -Ga₂O₃ has emerged as one of the most promising UWBG materials due to its unique combination of properties and manufacturing advantages [24]. With a bandgap of 4.9 eV and a critical electric field of 8 MV/cm, β -Ga₂O₃ exhibits a Baliga Figure of Merit (BFOM) more than 3000× that of silicon, suggesting tremendous potential for high-voltage power devices.

A key advantage of β -Ga₂O₃ is its compatibility with melt-growth techniques including the Floating Zone (FZ), Czochralski (CZ), and Edge-defined Film-fed Growth (EFG) methods. These methods enable production of large-diameter, high-quality single-crystal substrates at potentially lower costs than the vapor-phase growth required for SiC and GaN substrates. Currently, 2-inch substrates are commercially available from multiple suppliers, with 4-inch substrates in limited commercial production and 6-inch substrates demonstrated in research laboratories [35]. While substrate manufacturing has reached commercial maturity, device technology remains at the validation stage (TRL 5–6 per Horizon 2020 definitions), reflecting the gap between substrate availability and device qualification for end-use applications.

However, β -Ga₂O₃ faces two fundamental challenges. First, its relatively low thermal conductivity (0.1–0.3 W/cm·K) is approximately 10–30× lower than SiC, necessitating sophisticated thermal management solutions including heterogeneous integration with high-thermal-conductivity substrates. Second, the absence of effective p-type doping limits device architectures to unipolar configurations such as Schottky Barrier Diodes (SBDs) and Field-Effect Transistors (FETs). Recent research has explored heterostructures with NiO_x and other p-type materials to enable bipolar operation [36].

The global market for high-purity β -Ga₂O₃ power devices is projected to grow at a Compound Annual Growth Rate (CAGR) of approximately 24.5% from 2024 to 2033, with applications initially targeting the 600 V–3.3 kV range for EV power systems, solar inverters, and grid interface equipment.

3.2. Aluminum Nitride (AlN)

Aluminum nitride possesses the highest critical electric field (15 MV/cm) among practical UWBG semiconductors, enabling exceptionally thin drift regions and low on-resistance for a given breakdown voltage [37]. Its bandgap of 6.2 eV and Johnson's Figure of Merit 5× higher than GaN make it particularly attractive for both high-power switching and high-frequency applications.

A major breakthrough was reported at the IEEE International Electron Devices Meeting (IEDM) in December 2023, where researchers from Nagoya University demonstrated AlN-based diodes capable of withstanding electric fields of 7.3 MV/cm—approximately twice the capability of SiC or GaN [37]. This achievement utilized the Distributed Polarization Doping (DPD) technique, which enables effective n-type and p-type doping in AlGaN alloys without conventional impurity dopants, circumventing AlN's historically problematic doping challenges.

In 2024, a German research consortium led by Fraunhofer IISB successfully demonstrated a complete value chain for AlN-based devices in Europe [37]. The consortium grew AlN crystals up to 43 mm diameter, processed them into polished wafers, and fabricated AlN/GaN high-electron-mobility transistors (HEMTs) with breakdown voltages up to 2200 V and power densities superior to both SiC and GaN devices. These AlN/GaN HEMTs offer up to 3000× lower conduction losses than silicon and are approximately 10× more efficient than SiC transistors.

Crystal IS has achieved production of 100 mm (4-inch) diameter single-crystal AlN substrates with 99% usable area, a significant milestone toward commercial viability [37]. Researchers at Nagoya University project commercialization of AlN-based power devices in the 2030s, contingent on resolving remaining challenges in ohmic contact formation and scaling manufacturing processes.

3.3. Diamond

Diamond represents the ultimate semiconductor material, offering an unparalleled combination of an ultra-wide bandgap (5.5 eV), the highest thermal conductivity of any material (22–23 W/cm·K), exceptional carrier mobility (4500 cm²/Vs for electrons, 3800 cm²/Vs for holes), and a theoretical critical electric field of 10–20 MV/cm [23]. These properties yield a BFOM 50,000× that of silicon, positioning diamond as the long-term solution for extreme power density applications.

Significant progress has been made in diamond device development. Researchers at the University of Illinois Urbana-Champaign demonstrated diamond Schottky barrier diodes with the highest reported breakdown voltage (4.6 kV at 0.01 mA/mm) and lowest leakage current among diamond devices [23]. Japan's National Institute for Materials Science (NIMS) achieved another milestone in 2024 with the world's first n-channel diamond MOSFET, exhibiting field-effect mobility over 150 cm²/Vs at 573 K—the highest among all n-channel MOSFETs based on wide-bandgap semiconductors [23].

Japanese institutions are leading diamond semiconductor commercialization efforts. Saga University developed the world's first diamond-based power device in 2023 in collaboration with the Japan Aerospace Exploration Agency (JAXA) for high-frequency space communication applications. Orbray has developed mass-production technology for 2-inch diamond wafers and is progressing toward 4-inch substrates, with partnerships including Toyota and Denso supporting onboard power device development expected in the 2030s [23].

Diamond's primary challenges include the difficulty of n-type doping due to high activation energies, the lack of a mature manufacturing ecosystem, and substrate availability limitations. However, advances in chemical vapor deposition (CVD) growth and recent n-channel MOSFET demonstrations suggest these barriers are being systematically addressed.

3.4. Cubic Boron Nitride (c-BN)

Cubic boron nitride represents a compelling UWBG semiconductor that combines many of diamond's exceptional properties with potentially superior doping characteristics [38,39]. With a bandgap of 6.4 eV—the highest among practical semiconductors—and a theoretical critical electric field of 12 MV/cm, c-BN offers extraordinary high-voltage capability. Its thermal conductivity of 13 W/cm·K, while lower than diamond, significantly exceeds that of SiC and GaN.

The key advantage of c-BN over diamond lies in its doping flexibility. Both n-type and p-type doping have been demonstrated with activation energies lower than those in diamond, potentially enabling efficient bipolar devices [38]. Silicon substituting on the boron site (Si_B) serves as an effective n-type dopant, while beryllium and magnesium provide p-type conductivity. Recent work at North Carolina State University demonstrated n-type conductivity with carbon doping concentrations ranging from 2×10^{19} to 7×10^{21} cm⁻³, achieving semiconductor-like resistivity profiles [40].

Manufacturing c-BN remains challenging. Conventional High-Pressure, High-Temperature (HPHT) synthesis at >1,150°C and >2.5 GPa produces only millimeter-scale crystals—far below the centimeter-scale wafers required for electronics manufacturing [39]. However, breakthrough fabrication techniques are emerging:

Pulsed Laser Annealing (PLA): Researchers have demonstrated direct conversion of hexagonal BN (h-BN) into phase-pure single-crystal c-BN using nanosecond laser pulses, achieving conversion in approximately 200 ns at ambient pressure [41]. This technique can produce epitaxial c-BN thin films on sapphire substrates with controlled doping.

Solution growth: Texas Tech University, with Department of Energy (DOE) funding, is developing autoclave-based solution growth methods that could enable scalable production of electronic-grade c-BN wafers for extreme-temperature electronics [38].

Diamond/c-BN heterostructures: First-principles calculations indicate that diamond/c-BN heterojunctions can form high-density two-dimensional carrier gases at the interface, potentially enabling high-frequency, high-power devices that leverage both materials' advantages [42].

The projected applications for c-BN power devices include ultra-high-voltage (>10 kV) grid infrastructure, extreme-environment electronics for aerospace and geothermal applications, and next-generation smart grid transformers. While commercialization remains in the ≥ 2035 timeframe, c-BN's combination of UWBG properties and doping flexibility positions it as a potential ultimate solution for extreme power electronics.

Table 6 summarizes the development status and projected commercialization timeline for UWBG materials.¹

Table 6. UWBG Materials Development Status and Commercialization Timeline.

Parameter	$\beta\text{-Ga}_2\text{O}_3$	AlN	c-BN	Diamond
Wafer Size (Comm.)	4-inch ^a	4-inch	N/A	2-inch
Best Device V_{BR}	2.3 kV	2.2 kV	N/A	4.6 kV
TRL Level ^b	5–6	3–4	2–3	3–4
E_g (eV)	4.9	6.2	6.4	5.5
κ (W/cm·K)	0.1–0.3	2.85	13	22–23
Primary Challenge	Low κ	Doping/Contacts	Substrate size	n-type doping
Target Applications	600V–3.3kV	10kV+, RF	>10kV, extreme	Extreme power
Projected Commerc. ^c	2027–2030	2030–2035	≥ 2035	2030–2035

^a 4-inch substrates in limited commercial production; 2-inch widely available.

^b TRL per Horizon 2020 Work Programme (European Commission, 2014): TRL 5 = technology validated in relevant environment; TRL 6 = technology demonstrated in relevant environment.

^c Projected dates represent estimated initial commercial device availability; confidence decreases for longer-term projections.

4. WBG Device Architectures: SiC and GaN

The commercial landscape of WBG semiconductors has matured significantly [43,44]. This section presents device configurations for both SiC and GaN technologies.

4.1. SiC Device Configurations

Silicon Carbide power devices have evolved into several mature device architectures, each offering distinct advantages for specific application requirements [5,17]. Figure 6 presents the classification of commercial SiC power devices. SiC power devices are categorized into unipolar devices (MOSFETs, JFETs, and SBDs) and bipolar devices (BJTs, thyristors, and IGBTs), with unipolar devices dominating commercial applications due to their superior switching characteristics and reduced reverse recovery losses.

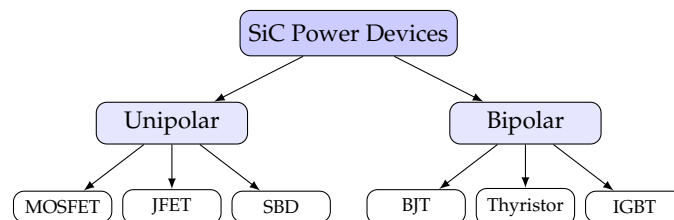


Figure 6. Classification of SiC power devices

4.1.1. SiC MOSFET Structure

The SiC MOSFET is the dominant commercial device, offering normally-off operation with voltage-controlled switching [45]. The planar MOSFET suffers from the “JFET effect”—the narrow

¹ Technology Readiness Levels (TRL) follow the Horizon 2020 Work Programme definitions (European Commission, 2014–2020): TRL 1–3 (research), TRL 4–6 (development/validation), TRL 7–9 (demonstration/deployment).

conduction path between adjacent p-wells increases on-resistance. Trench MOSFETs eliminate this limitation by orienting the channel vertically, achieving 30–50% lower specific on-resistance [46]. The on-resistance of a SiC MOSFET can be expressed as:

$$R_{DS(on)} = R_{ch} + R_{JFET} + R_{drift} + R_{sub} + R_{contact} \quad (7)$$

where R_{ch} is channel resistance, R_{JFET} is the JFET region resistance (eliminated in trench designs), R_{drift} is drift region resistance, R_{sub} is substrate resistance, and $R_{contact}$ represents contact resistances. Figure 7 illustrates the planar and trench SiC MOSFET structures. The planar SiC MOSFET features a horizontal channel with gate oxide on the semiconductor surface, while the trench MOSFET incorporates a vertical channel structure with the gate embedded within a trench, enabling higher channel density and lower on-resistance at the cost of increased gate oxide electric field stress.

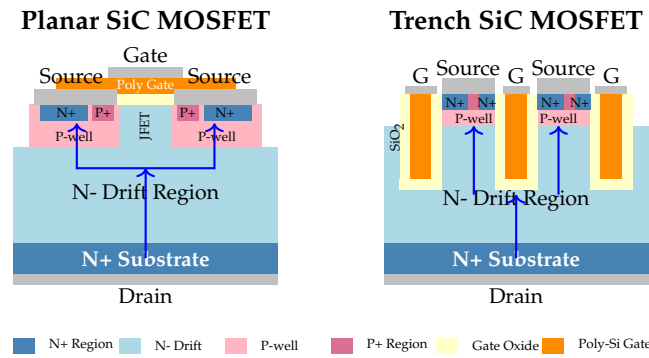


Figure 7. Planar SiC MOSFET and Trench SiC MOSFET Structures

4.2. SiC Device Selection Criteria and Loss Models

The selection of SiC MOSFETs for power converter applications requires evaluation of key physical parameters and their impact on system performance. The fundamental selection criteria include:

Breakdown Voltage (V_{BR}): SiC devices are commercially available with ratings from 650 V to 1700 V. The drift region resistance scales with blocking voltage as $R_{drift} \propto V_{BR}^{2.5} / \mu_n \epsilon E_c^3$, where μ_n is electron mobility, ϵ is permittivity, and E_c is critical electric field (2.2–3 MV/cm for SiC).

On-State Resistance ($R_{DS(on)}$): Total on-resistance comprises channel and drift components: $R_{DS(on)} = R_{ch} + R_{drift}$. SiC exhibits positive temperature coefficient above 25°C, enabling natural current sharing in parallel configurations.

Switching Frequency (f_{sw}): SiC MOSFETs typically operate at 20–150 kHz in hard-switching applications. Gate charge Q_g and output capacitance C_{oss} determine switching speed capability.

Power Loss Models: Total device losses comprise conduction and switching components:

$$P_{total} = P_{cond} + P_{sw} = I_{D,rms}^2 \cdot R_{DS(on)} + (E_{on} + E_{off}) \cdot f_{sw} \quad (8)$$

Switching energy can be estimated analytically from datasheet parameters:

$$E_{on} \approx \frac{1}{2} V_{DS} \cdot I_D \cdot (t_{ri} + t_{fu}) + Q_{rr} \cdot V_{DS} \quad (9)$$

$$E_{off} \approx \frac{1}{2} V_{DS} \cdot I_D \cdot (t_{ru} + t_{fi}) \quad (10)$$

where t_{ri} , t_{fu} , t_{ru} , t_{fi} are current rise, voltage fall, voltage rise, and current fall times, respectively, and Q_{rr} is reverse recovery charge.

Gate Drive Requirements: Recommended gate voltage is $V_{GS} = +15$ to $+20$ V (on) and -2 to -5 V (off). The Miller plateau voltage V_{Miller} determines the voltage fall/rise duration during switching transitions.

Thermal Considerations: Junction-to-case thermal resistance $R_{th,jc}$ and maximum junction temperature $T_{j,max}$ (typically 175–200°C) define power density limits. Thermal impedance $Z_{th}(t)$ is critical for pulsed operation.

4.3. GaN Device Configurations

Figure 8 presents the classification of GaN HEMT devices. GaN power devices are categorized into GaN-on-Si structures using E-Mode and D-Mode HEMTs (with discrete or cascode configurations) and GaN-on-GaN structures utilizing V-GaN FETs, where GaN-on-Si dominates commercial markets due to cost advantages while GaN-on-GaN offers superior performance through reduced substrate-related defects.

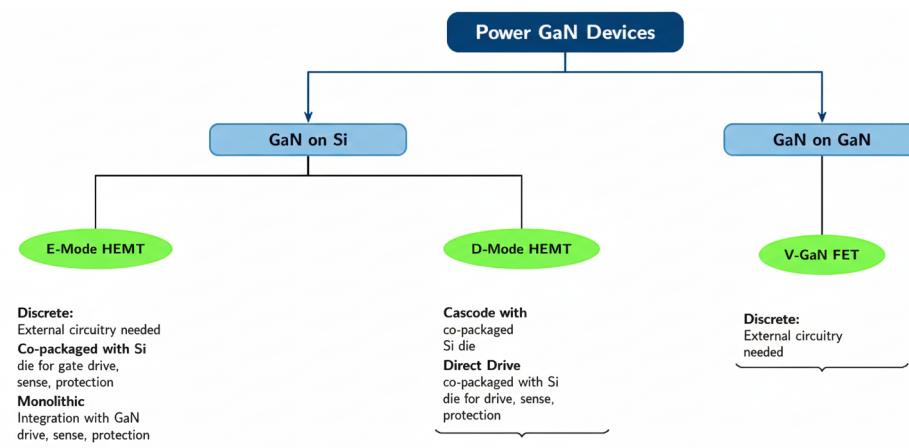


Figure 8. Classification of GaN HEMTs devices.

Figure 9 illustrates the different types of GaN devices including normally-on and normally-off configurations. The figure shows the evolution from D-Mode (normally-on) GaN HEMTs to E-Mode (normally-off) configurations through various enhancement techniques, including cascode configurations that combine low-voltage Si MOSFETs with high-voltage D-Mode GaN devices to achieve normally-off operation with improved gate drive compatibility.

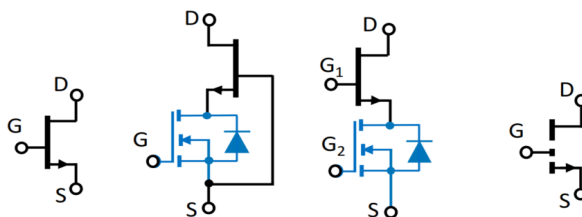


Figure 9. Different types of GaN devices: Normally-on (d-mode), Normally-off Cascode (d-mode), Direct Drive (d-mode), Normally off (e-mode)

4.3.1. Depletion-Mode (D-Mode) GaN HEMTs

D-mode devices are inherently normally-on, requiring a negative gate voltage to turn off. The Two-Dimensional Electron Gas (2DEG) at the AlGa_xGaN/GaN interface provides exceptionally high electron mobility and carrier density. Figure 10 shows the internal structure of a D-mode GaN HEMT, as described in detail in [47,48].

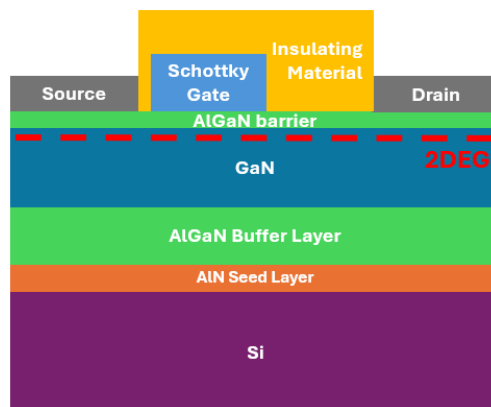


Figure 10. GaN D-Mode Internal Structure

4.3.2. Enhancement-Mode (E-Mode) GaN HEMTs

E-mode devices achieve normally-off operation through p-doped GaN gate structures [49,50]. This configuration is preferred for power electronics applications due to inherent safety during start-up and fault conditions. Figure 11 shows the internal structure as described in detail in [47].

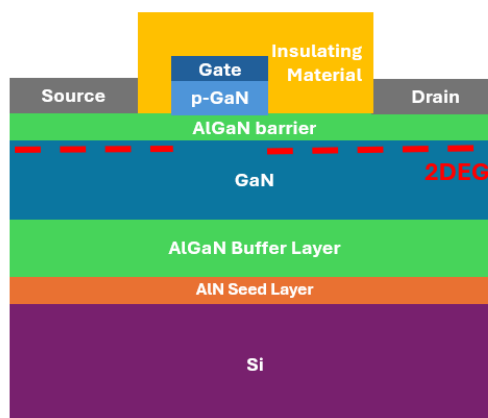


Figure 11. GaN E-Mode Internal Structure

4.4. GaN Device Selection Criteria and Loss Models

GaN HEMTs offer distinct advantages for high-frequency power conversion, requiring specific selection criteria:

Breakdown Voltage (V_{BR}): Commercial GaN HEMTs are rated at 100–650 V, with emerging devices reaching 1200 V. The lateral structure and 2DEG channel provide high electron mobility ($\sim 2000 \text{ cm}^2/\text{V}\cdot\text{s}$) enabling low $R_{DS(on)}$.

On-State Resistance ($R_{DS(on)}$): GaN exhibits positive temperature coefficient, with $R_{DS(on)}(T) = R_{DS(on),25} \cdot (T_j/298)^\alpha$, where $\alpha \approx 1.5\text{--}2.0$. Dynamic $R_{DS(on)}$ increase due to charge trapping must be considered in loss calculations.

Switching Frequency (f_{sw}): GaN HEMTs enable MHz-range operation (1–10 MHz) due to significantly lower gate charge (Q_g typically 5–15 nC) and output charge (Q_{oss}) compared to SiC, achieving 10 \times reduction versus equivalent Si devices.

Power Loss Models: For high-frequency GaN applications, capacitive losses become significant:

$$P_{total} = I_{D,rms}^2 \cdot R_{DS(on)} + (E_{on} + E_{off}) \cdot f_{sw} + E_{oss} \cdot f_{sw} \quad (11)$$

where $E_{oss} = \int_0^{V_{DS}} C_{oss}(v) \cdot v \, dv$ represents output capacitance energy loss.

Conduction losses dominate in GaN converters due to reduced switching losses, for example considering a buck converter:

$$P_{cond} = D \cdot I_D^2 \cdot R_{DS(on)} + (1 - D) \cdot I_D \cdot V_F \quad (12)$$

where D is duty cycle and V_F is body diode (or anti-parallel diode) forward voltage.

Gate Drive Requirements: Enhancement-mode GaN HEMTs require $V_{GS} = +5$ to $+6$ V (on) and 0 V (off), with maximum V_{GS} typically limited to 7 V. Negative turn-off voltage (-3 V) is recommended to prevent spurious turn-on from dv/dt induced gate charging.

Thermal Considerations: GaN-on-Si devices have $T_{j,max} = 150$ – 175°C . The lateral heat spreading and thermal boundary resistance at the GaN/substrate interface require careful PCB thermal design with thermal vias directly beneath the device.

Power Density: GaN enables power densities exceeding 100 W/in³ due to reduced passive component size at high frequencies, with inductor volume scaling approximately as $V_L \propto 1/f_{sw}$ [5].

4.5. Vertical GaN Power Devices

While lateral GaN HEMTs dominate the commercial market for voltages up to 650 V, vertical GaN devices are emerging as critical enablers for medium-voltage applications (1.2 – 10 kV) where they compete directly with SiC [51]. Unlike lateral devices where voltage scaling requires proportionally larger chip area, vertical GaN conducts current perpendicular to the substrate surface, allowing breakdown voltage to increase through drift layer thickness while maintaining compact chip dimensions.

Recent advances have demonstrated impressive performance milestones. Vertical GaN (vGaN) technology features $1,200$ V-class devices capable of reducing system losses by nearly 50% compared to lateral GaN, while achieving approximately $3\times$ smaller die size [51]. Vertical GaN transistors with operating currents exceeding 50 A have been demonstrated, enabling MHz-frequency operation in compact packages [51].

Vertical GaN architectures include trench MOSFETs (T-MOSFETs), Current Aperture Vertical Electron Transistors (CAVETs), and vertical Junction Field-Effect Transistors (JFETs). The 1.2 kV vertical GaN fin-channel JFET has emerged as a particularly promising device, offering normally-off operation, avalanche capability, and no dynamic R_{on} degradation—addressing one of the primary reliability concerns of lateral GaN HEMTs [52].

Key challenges for vertical GaN include the limited availability of native GaN substrates (currently 2 – 4 inch), high substrate costs, and the difficulty of achieving low background doping ($< 1.5 \times 10^{16}$ cm⁻³) in thick drift layers required for 1.2 kV+ operation. However, advances in GaN-on-engineered-substrate technology are enabling 200 mm CMOS-compatible fabrication pathways that could dramatically reduce costs [53].

4.6. GaN Bidirectional Switches (BDS)

Monolithic bidirectional switches represent a paradigm shift in power semiconductor technology, enabling four-quadrant operation—bidirectional current flow and bipolar voltage blocking—from a single device [43]. While conventional approaches require four discrete transistors in back-to-back configurations (doubling $R_{DS(on)}$ and component count), GaN BDS devices leverage the lateral HEMT structure to integrate two opposing gates sharing a common drift region. An example is provided in the following Section 5.1.2.

Commercial GaN BDS devices offer ratings at 40 V, 650 V, and 850 V with four operational modes: full conduction, full blocking, and two diode modes (forward and reverse blocking) [43].

Key applications for GaN BDS include matrix converters (direct AC-AC conversion without DC-link), Vienna rectifiers (three-level PFC with bidirectional current capability), T-type inverters (three-level topologies for solar and motor drive applications), Current-Source Inverters (CSI) for high-power motor drives and High-Voltage Direct Current (HVDC) transmission, and Highly Efficient

and Reliable Inverter Concept (HERIC) inverters for Photovoltaic (PV) applications with reactive power capability.

Table 7 summarizes the key differences between WBG device technologies. GaN HEMTs offer the best switching speed (1–40 MHz) and minimal reverse recovery losses with low on-resistance (1–5 mΩcm²), while SiC MOSFETs provide superior high-voltage capability (650–3300 V) and higher current ratings (5–200 A), and Si IGBTs remain cost-effective for high-power applications despite significantly slower switching speeds (0.02–0.1 MHz) and poor reverse recovery characteristics.

Table 7. Comparison of WBG and Si Device Characteristics, data taken from [4,43].

Parameter	GaN HEMT	GaN Cas.	SiC MOS	Si IGBT
Voltage (V)	600–650	600–900	650–3300	600–6500
Current (A)	1–90	10–60	5–200	10–3600
$R_{on} \cdot A$ (mΩcm ²)	1–5	3–8	3–15	—
Max f_{sw} (MHz)	1–40	0.5–10	0.1–2	0.02–0.1
dv/dt (V/ns)	50–200	30–100	20–100	1–20
Q_g (nC)	1–20	10–50	20–300	100–5000
Max T_j (°C)	150–175	150	175–200	175
Rev. Recovery	None	Limited	Moderate	V. High
FOM ($R \cdot Q$)	Best	Good	Good	Poor
Cost (\$/A)	Medium	Med-High	High	Low

5. Converter Topologies for WBG Devices

5.1. SiC Converter Topologies

SiC devices excel in high-power, high-voltage converter applications where their superior breakdown voltage and thermal conductivity provide significant advantages over both Si and GaN alternatives [17].

5.1.1. Three-Phase Traction Inverter

The three-phase voltage source inverter is the dominant topology for electric vehicle traction drives [54]. Figure 12 shows a SiC-based traction inverter configuration. The three-phase voltage source inverter (VSI) topology consists of six SiC MOSFETs (M_1 – M_6) arranged in three half-bridge legs with a DC-link capacitor (C_{DC}), enabling bidirectional power flow and efficient motor control for electric vehicle traction applications.

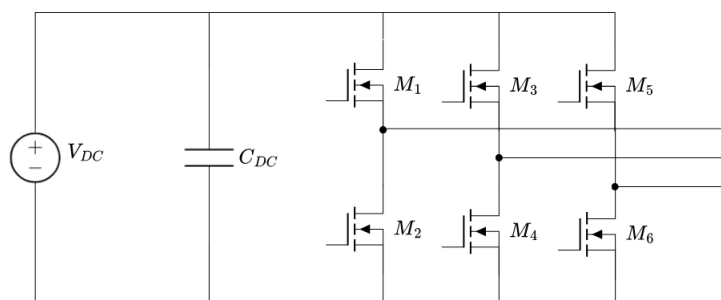


Figure 12. SiC-based three-phase traction inverter for electric vehicle applications, adapted from [55].

The power loss in each SiC MOSFET comprises conduction and switching components:

$$P_{loss} = I_{rms}^2 \cdot R_{DS(on)}(T_j) + f_{sw}(E_{on} + E_{off}) \quad (13)$$

SiC enables switching frequencies of 10–20 kHz in traction applications (versus 5–10 kHz for Si IGBTs), reducing motor current ripple and acoustic noise while maintaining >98% inverter efficiency [12].

5.1.2. DC Fast Charging Converter

DC fast charging stations (50–350 kW) leverage SiC's high-voltage capability and efficiency [56]. Figure 13 shows a typical three-phase Vienna rectifier front-end with isolated DC-DC stage. The topology combines a three-phase Vienna rectifier for AC/DC conversion with bidirectional switches and diodes for power factor correction, followed by isolated DC/DC converter stages that provide galvanic isolation and voltage regulation for EV battery charging applications.

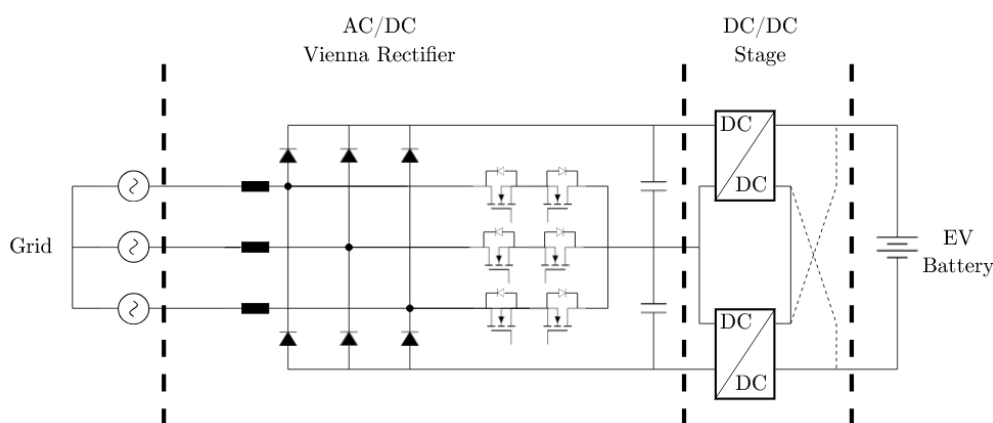


Figure 13. SiC-based DC fast charging architecture: Vienna rectifier PFC front-end with isolated DC-DC converter, adapted from [26].

The Vienna rectifier achieves near-unity power factor with reduced switch count compared to conventional Pulse Width Modulation (PWM) rectifiers, while SiC enables operation at 30–50 kHz for compact magnetic design.

5.1.3. Grid-Tied Solar Inverter

Central and string inverters for photovoltaic applications benefit from SiC's efficiency at partial load conditions [57]. Figure 14 shows a three-level T-type inverter topology. The configuration features a DC-link with split capacitors and bidirectional switches in each phase leg, enabling three-level voltage output that reduces harmonic distortion and improves efficiency for grid-tied solar PV applications through reduced dv/dt stress and lower filtering requirements.

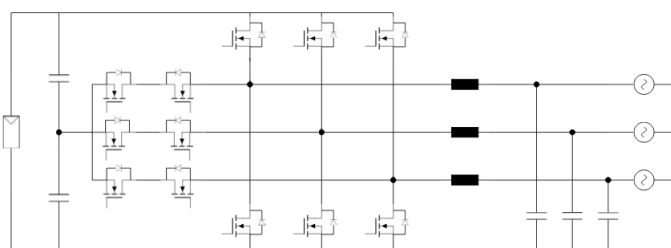


Figure 14. SiC-based T-type three-level inverter for grid-tied PV applications, adapted from [57]

Three-level topologies reduce the voltage stress on each device to $V_{DC}/2$, enabling higher DC-link voltages (up to 1500 V for utility-scale installations) while maintaining acceptable dv/dt levels. The output voltage Total Harmonic Distortion (THD) is significantly improved:

$$THD_{3L} \approx \frac{THD_{2L}}{2} \quad (14)$$

5.2. GaN Converter Topologies

Implementing GaN devices in power converter topologies requires careful consideration of their unique characteristics [58,59]. Printed Circuit Board (PCB) layout is critical for achieving optimal performance.

5.2.1. Buck Converters

The synchronous buck converter represents an ideal topology for demonstrating GaN advantages [18]. The inductance value is selected to maintain Continuous Conduction Mode (CCM) operation [60]:

$$L = \frac{V_{out}(V_{in} - V_{out})}{V_{in} \cdot f_{sw} \cdot \Delta I_L} \quad (15)$$

Output voltage ripple is given by:

$$\Delta V_{out} = \Delta I_L \cdot \text{ESR} + \frac{\Delta I_L}{8f_{sw}C_{out}} \quad (16)$$

5.2.2. Interleaved Buck Converters

Interleaving multiple phases provides significant advantages in high-current applications [61]. The current imbalance between phases is [60]:

$$\Delta I_{imbalance} = I_{out} \cdot \frac{\Delta L/L + \Delta R_{DS(on)}/R_{DS(on)}}{N} \quad (17)$$

5.2.3. Dual Active Bridge Converters

The DAB converter has emerged as a leading topology for bidirectional isolated DC-DC conversion [62–64]. Zero Voltage Switching (ZVS) operation is achievable over a wide load range. The average power transfer is [65]:

$$P = \frac{nV_1V_2}{2\pi f_s L_s} \phi \left(1 - \frac{|\phi|}{\pi}\right) \quad (18)$$

The inductor current evolution is:

$$i_{L_s}(t) = i_{L_s}(0) + \frac{1}{L_s} \int_0^t v_{L_s}(\tau) d\tau \quad (19)$$

5.2.4. Multilevel DAB Topologies

For medium-voltage applications (>1 kV), multilevel DAB topologies extend capabilities [16]. The three-level Neutral Point Clamped (NPC) DAB reduces voltage stress on individual switches:

$$V_{switch,3L} = \frac{V_{dc}}{2} < V_{switch,2L} = V_{dc} \quad (20)$$

5.3. GaN Technology Evolution: Vertical GaN and BDS for Converter Topologies

While the preceding sections focused on established SiC and lateral GaN technologies, this section examines how emerging GaN device architectures—specifically vertical GaN and monolithic bidirectional switches (BDS)—are reshaping converter design possibilities. Table 8 provides a topology-by-topology analysis of how these emerging technologies compare to established SiC solutions. Vertical GaN devices promise 50–100 kHz operation with reduced losses for traction inverters and enhanced

switching speed for T-type inverters, while GaN BDS technology offers transformative advantages including single-device solutions for Vienna rectifiers and DAB converters, MHz operation for HERIC inverters, native bidirectional blocking for motor drives, and elimination of DC-link capacitors in single-stage OBC designs, with commercial availability expected between 2025–2029.

5.3.1. Vertical GaN: Challenging SiC in Medium-Voltage Applications

Vertical GaN power devices represent a paradigm shift from traditional lateral GaN-on-Si HEMTs, enabling operation at 1.2 kV and beyond—voltage classes currently dominated by SiC [51,53]. Unlike lateral devices where breakdown voltage scales with chip area, vertical GaN conducts current perpendicular to the substrate, allowing voltage scaling through drift layer thickness while maintaining compact die dimensions.

Topology Implications:

Three-Phase Traction Inverters: The traditional domain of SiC MOSFETs, traction inverters are a prime target for vertical GaN. Onsemi's 1,200 V vGaN technology demonstrates nearly 50% lower losses compared to lateral GaN and approximately $3\times$ smaller die size [52]. The superior switching figure of merit ($R_{on} \times Q_g$) enables switching frequencies of 50–100 kHz while maintaining efficiency above 99%, compared to 10–20 kHz typical for SiC traction inverters. The reduced Q_{oss} also simplifies soft-switching in resonant topologies.

DC Fast Charging (Vienna Rectifier and DAB): For 800 V battery systems, 1.2 kV vertical GaN enables single-device implementations without series stacking. The absence of dynamic R_{on} degradation—a key reliability concern in lateral GaN HEMTs [66]—makes vertical GaN particularly attractive for high duty-cycle applications like DC fast chargers.

Grid-Tied Inverters: Medium-voltage applications (1500 V DC-link for utility-scale PV) require 3.3 kV device ratings. Vertical GaN development is progressing toward this voltage class, with 2.3 kV demonstrations reported in research [53]. When commercially available, vertical GaN could challenge SiC in this application through superior switching speed.

Key Advantages over Lateral GaN:

- Voltage scaling through drift layer thickness rather than lateral area
- No dynamic R_{on} degradation (no surface traps)
- Avalanche capability similar to SiC MOSFETs
- Reduced chip area for given voltage/current rating

Current Limitations:

- Limited substrate availability (2–4 inch GaN-on-GaN)
- Higher substrate cost compared to SiC or GaN-on-Si
- Manufacturing maturity gap (TRL 4–5 vs. TRL 8–9 for SiC)
- Projected commercialization: 2026–2028 for 1.2 kV class

5.3.2. Bidirectional GaN Switches: Enabling Single-Stage Power Conversion

Monolithic bidirectional switches (BDS) represent perhaps the most transformative GaN innovation for power converter topologies [8,26]. By integrating four-quadrant operation (bidirectional current flow and bipolar voltage blocking) into a single device, GaN BDS enables entirely new converter architectures previously impractical with discrete devices.

Revolutionary Topology Enablement:

Single-Stage AC-DC Conversion: Traditional two-stage converters (PFC + isolated DC-DC) require intermediate DC-link capacitors—often the largest, heaviest, and least reliable components. GaN BDS enables single-stage isolated conversion through cycloconverter and matrix-type topologies, eliminating the DC-link entirely [26]. Benefits include:

- 40–50% size reduction in EV on-board chargers
- Elimination of electrolytic capacitors (improved reliability)
- Inherent bidirectional power flow (V2G capability)

- Higher efficiency through single-stage conversion

Matrix Converters (Direct AC-AC): Matrix converters provide direct frequency conversion without DC-link, but historically required complex discrete switch arrays. Each bidirectional switch position previously needed four discrete transistors in anti-series/anti-parallel configuration, quadrupling component count and on-resistance. A single GaN BDS replaces this four-device array, making matrix converters practical for:

- Variable-frequency motor drives
- Solid-state transformers
- Grid frequency conversion

Vienna Rectifiers and T-Type Inverters: These three-level topologies require bidirectional switches for the neutral-point connection. Replacing back-to-back discrete switches with GaN BDS provides:

- 50% reduction in on-resistance for bidirectional current path
- Simplified gate drive (two isolated channels vs. four)
- Higher switching frequency capability (>100 kHz vs. 30–50 kHz)
- Reduced PCB complexity and parasitic inductance

HERIC Inverters for PV: The HERIC topology uses bidirectional switches to decouple the PV array from the grid during freewheeling periods, reducing common-mode leakage current. GaN BDS enables MHz-frequency operation of HERIC inverters while supporting reactive power compensation for grid support functions.

Current-Source Inverters (CSI): CSI topologies require bidirectional voltage blocking, traditionally achieved with series diodes that increase losses. GaN BDS provides native bidirectional blocking with lower on-resistance, enabling CSI adoption for high-power motor drives with improved efficiency and inherent short-circuit protection [18].

Table 8. GaN Technology Evolution: Impact on Converter Topologies vs. Established SiC.

Topology	Current SiC Solution	Vertical GaN Potential	GaN BDS Potential	Timeline
Traction Inverter	1.2 kV SiC MOSFET, 10–20 kHz	1.2 kV vGaN, 50–100 kHz, 50% lower losses	Not applicable	vGaN: 2027–2029
Vienna Rectifier	Back-to-back SiC, 30–50 kHz	Higher frequency, smaller magnetics	Single-device solution, 100 kHz+	BDS: 2025–2026
DAB Converter	SiC for >50 kW, ZVS operation	Smaller transformer, higher frequency	Single-stage capability	vGaN: 2028+
T-Type Inverter	Discrete SiC neutral switches	Enhanced switching speed	50% lower R_{on} , simplified drive	BDS: Available now
Matrix Converter	Complex discrete arrays	N/A	Revolutionary: single-device BDS	BDS: 2025–2026
HERIC (PV)	Discrete Si/SiC switches	N/A	MHz operation, grid support	BDS: Available now
CSI Motor Drive	SiC + series diodes	Native blocking, lower losses	Native bidirectional blocking	Both: 2027+
Single-Stage OBC	Two-stage (PFC + DC-DC)	N/A	Eliminates DC-link capacitor	BDS: 2025–2026

5.3.3. Design Guidelines for Technology Selection

Based on the analysis of current SiC capabilities and emerging GaN technologies, the following guidelines assist designers in technology selection.

SiC remains the preferred choice when voltage requirements exceed 1.2 kV (until vertical GaN matures), when high current capability above 100 A with an established supply chain is required, or when short-circuit withstand capability is critical. Additionally, SiC should be selected for applications

demanding junction temperatures exceeding 175°C or where proven reliability and qualification data are mandatory.

Vertical GaN should be considered for designs targeting the 2027+ timeframe when maximum switching frequency above 50 kHz provides meaningful benefits, when power density represents the primary optimization target, or when dynamic $R_{ds,on}$ stability is critical for continuous hard-switching operation. This technology is also attractive when avalanche capability combined with superior switching FOM is desired, particularly for voltage classes between 650 V and 1.2 kV.

GaN BDS technology is recommended when bidirectional current flow and voltage blocking are required, when single-stage conversion topology is feasible, or when DC-link capacitor elimination offers significant advantages in terms of size, reliability, or cost. This technology is particularly well-suited for Vienna, T-type, HERIC, or matrix topologies, for applications targeting switching frequencies above 100 kHz, and for grid-connected systems requiring reactive power support.

5.3.4. Market and Technology Outlook

The convergence of vertical GaN and BDS technologies is expected to accelerate the displacement of SiC in specific application segments while opening entirely new topology possibilities. Key milestones include:

- **2025:** Commercial 650 V GaN BDS devices (Infineon, Navitas); initial vertical GaN sampling at 700–1200 V
- **2026–2027:** Production vertical GaN for EV traction; BDS adoption in solar microinverters
- **2028–2030:** Vertical GaN challenging SiC in medium-voltage segments; matrix converters becoming mainstream
- **2030+:** Potential vertical GaN extension to 3.3 kV for grid applications

The combination of vertical GaN for high-voltage unidirectional applications and BDS for bidirectional topologies positions GaN technology as a comprehensive competitor to SiC across the medium-voltage power electronics landscape, rather than remaining confined to the sub-650 V market segment.

6. SiC vs. GaN: Comprehensive Comparison

6.1. Topology-Specific Comparison

The selection between SiC and GaN devices depends critically on the converter topology, power level, voltage class, and switching frequency requirements. Table 12 provides a comprehensive comparison for the major power converter topologies. SiC devices are recommended for high-power applications (>100 kW two-level VSI, >10 kW buck, >50 kW DAB, >30 kW Vienna rectifiers) due to superior voltage ratings (1.2–3.3 kV) and current handling, while GaN excels in low-to-medium power applications (<1 kW buck, <20 kW DAB, T-type/NPC, LLC resonant) with advantages including 10× lower Q_g , MHz switching operation, smaller magnetics, and significantly reduced output capacitance enabling phase current cancellation.

Table 9. SiC vs. GaN Comparison for Major Power Converter Topologies.

Topology	SiC Advantages	GaN Advantages	Recommended
Two-Level VSI	Higher voltage (1.2–3.3 kV), better thermal	Lower switching losses, smaller passives	SiC (>100 kW)
Buck (<1 kW)	Better thermal margin	10× lower Q_g , MHz operation	GaN
Buck (>10 kW)	Higher current handling	Lower switching losses at 100–500 kHz	SiC
Interleaved	Better current sharing, thermal stability	Phase current cancellation, smaller magnetics	Application dependent
DAB (<20 kW)	Wide ZVS range	>500 kHz, smaller transformer	GaN
DAB (>50 kW)	1.2 kV/>100 A devices	Lower turn-off losses	SiC
Vienna Rectifier	Higher voltage margin	Lower THD with higher f_{sw}	GaN (<30 kW); SiC (>30 kW)
T-Type/NPC	1700 V devices for 1500 V PV	BDS enables single-package solution	GaN (resid.); SiC (utility)
LLC Resonant	Wide input range, stable C_{oss}	Very low C_{oss} , enables >1 MHz	GaN

6.2. Thermal Stability Considerations

Table 10. Thermal Properties of Wide-Bandgap Semiconductors for Power Electronics

Property	SiC (4H)	GaN	AlN
Thermal conductivity (W/m·K)	330–490	130–200	285–320
Max. junction temperature (°C)	>200	150–175	>200
Bandgap (eV)	3.26	3.4	6.2
Thermal coeff. of κ	$\sim T^{-1.26}$	Strongly negative	$\sim T^{-1}$

Table 10 summarizes the key thermal properties governing heat dissipation in wide-bandgap power devices. SiC exhibits superior thermal conductivity (330–490 W/m·K), approximately 3× higher than GaN (130–200 W/m·K), enabling reliable operation at junction temperatures exceeding 200°C with simplified thermal management. GaN’s thermal conductivity decreases significantly with temperature, creating a thermal management challenge: as device temperature rises under high-power operation, heat dissipation capability diminishes. This self-heating effect reduces carrier mobility, shifts threshold voltage, and approximately doubles failure rates for every 10°C increase in junction temperature, limiting practical GaN operation to 150–175°C. AlN offers thermal conductivity comparable to SiC (285–320 W/m·K) combined with a wider bandgap (6.2 eV), making it attractive as a buffer layer or substrate material to improve thermal performance in GaN-based devices.

From a practical standpoint, SiC remains preferred for high-power applications (>10 kW) where thermal conductivity dominates design constraints, enabling smaller heatsinks and simpler cooling solutions. GaN devices require more conservative thermal derating and advanced packaging approaches (double-sided cooling, embedded die) to compensate for lower thermal conductivity. These considerations reinforce the topology-dependent recommendations in Table 9, where SiC is favored for thermally demanding applications (Two-Level VSI >100 kW, Buck >10 kW) while GaN excels in high-frequency, medium-power applications where switching performance advantages outweigh thermal management complexity.

6.3. Efficiency and Loss Comparison

The total losses in a power converter include conduction and switching components. For a given topology, the device selection significantly impacts both:

Conduction losses: SiC MOSFETs exhibit positive temperature coefficient of $R_{DS(on)}$, improving current sharing in parallel configurations but increasing losses at elevated temperatures. GaN HEMTs have flatter temperature dependence and lower specific on-resistance ($R_{on} \cdot A$) below 650 V, but require more devices in parallel for high-current applications.

Switching losses: GaN devices achieve 3–10× lower switching energy (E_{sw}) than equivalently-rated SiC MOSFETs due to smaller gate charge and output capacitance. This advantage enables proportionally higher switching frequencies, reducing passive component size according to:

$$L_{min} \propto \frac{1}{f_{sw}}, \quad C_{min} \propto \frac{1}{f_{sw}} \quad (21)$$

6.4. Application-Specific Recommendations

Based on the comprehensive analysis, the following guidelines emerge:

EV Traction Inverter (>100 kW, 400–800 V): SiC MOSFET is the clear choice due to 1.2 kV voltage rating, superior thermal management, and proven reliability. GaN may enter this space with vertical GaN devices in the 2027–2030 timeframe.

On-Board Charger (3.3–22 kW): GaN preferred for 6.6–11 kW class where MHz switching enables significant size reduction. SiC competitive at 22 kW and above where thermal management dominates.

DC Fast Charging (>50 kW): SiC dominates due to 800–1000 V DC-link requirements and high power levels.

Server/Telecom PSU (1–3 kW): GaN preferred for highest power density and efficiency in space-constrained applications.

Solar String Inverter (5–20 kW): GaN increasingly competitive with SiC, offering efficiency >99% with smaller EMI filters. BDS-enabled single-stage topologies emerging.

Motor Drives (<10 kW): GaN enables higher PWM frequencies reducing motor losses and acoustic noise. Current-source inverters with GaN BDS offer EMI advantages.

6.5. Gate Driver Requirements

The fundamental differences between Si, SiC, and GaN devices necessitate distinct gate driver designs. The key factor differentiating WBG and Si driving characteristics is the much faster transient capability of WBG devices, requiring shorter driver rise/fall times and propagation delays [59]. Table 11 provides a comprehensive comparison of gate driver requirements. GaN HEMTs require the simplest gate drive circuitry with low gate charge (1–10 nC), minimal voltage swing (+5 to +6 V turn-on, 0 V turn-off), ultrafast switching (<20 ns propagation delay), and no negative bias requirement, while SiC MOSFETs demand higher gate voltages (+15 to +20 V), larger gate charge (20–100 nC), and mandatory negative bias (–3 to –5 V), and Si devices show the highest immunity (10–50 V/μs) but require substantial gate charge (50–500 nC).

Table 11. Gate Driver Requirements Comparison: Si vs. SiC vs. GaN, data taken from [8,27,59].

Parameter	Si MOSFET/IGBT	SiC MOSFET	GaN HEMT
V_{GS} Turn-on	+10 to +15 V	+15 to +20 V	+5 to +6 V
V_{GS} Turn-off	0 V	-3 to -5 V	0 V
Gate Charge (Q_g)	50–500 nC	20–100 nC	1–10 nC
Peak Drive Current	1–4 A	4–10 A	1–5 A
Propagation Delay	50–200 ns	20–50 ns	<20 ns
dV/dt Immunity	10–50 V/ns	50–150 V/ns	100–300 V/ns
Negative Bias Req.	Optional	Required	Not Required
Miller Plateau	Flat, defined	Higher, not flat	Low, fast
V_{th} Range	2–4 V	1.5–4 V	1–2 V

6.5.1. SiC MOSFET Gate Drive Considerations

SiC MOSFETs require careful gate drive optimization to achieve reliable high-speed switching [25]. The recommended gate-source voltage is typically +18 to +20 V for turn-on to minimize on-resistance, with -3 to -5 V for turn-off to ensure complete channel depletion and prevent spurious turn-on from dV/dt -induced Miller current. The non-flat Miller plateau characteristic of SiC MOSFETs, occurring at higher V_{GS} than silicon devices, is a consequence of the lower transconductance inherent to SiC. SiC devices also exhibit higher internal gate resistance ($R_{G,int}$), which can limit switching speed if the external gate driver impedance is not sufficiently low.

Key protection features for SiC gate drivers include desaturation detection with response times below 200 ns for short-circuit protection, active Miller clamping to prevent false turn-on during high dV/dt transients, and Under-Voltage Lockout (UVLO) for both positive and negative supply rails.

6.5.2. GaN HEMT Gate Drive Considerations

Enhancement-mode GaN HEMTs present unique gate drive challenges due to their low threshold voltage (typically 1–2 V), limited gate voltage range (maximum V_{GS} of 6–7 V), and extremely fast switching capability [27,59]. The gate structure in p-GaN HEMTs is essentially a forward-biased diode, which can conduct significant gate current if V_{GS} exceeds the forward voltage.

GaN devices benefit significantly from integrated gate drivers that minimize parasitic inductance in the gate loop. Products such as Navitas GaNSafe and EPC eGaN ICs integrate the gate driver with the power transistor in a single package, achieving zero gate-source loop inductance and enabling switching frequencies up to 2 MHz [18]. For discrete GaN implementations, the gate driver should be placed as close as possible to the device with minimal loop area, and Common-Mode Transient Immunity (CMTI) exceeding 100 V/ns is essential.

6.6. Topology-Level Comparison: V-GaN, BDS and SiC

Vertical GaN MOSFETs: Unlike lateral GaN HEMTs limited to ≤ 650 V, vertical GaN devices on bulk GaN substrates target 1.2–3.3 kV applications. The vertical architecture enables current flow perpendicular to the substrate, achieving breakdown voltages exceeding 1.2 kV with specific on-resistance $R_{on,sp}$ of 2–6 $m\Omega \cdot cm^2$. Key advantages include avalanche ruggedness and elimination of current collapse (dynamic $R_{DS(on)}$ degradation). However, $R_{on,sp}$ remains higher than SiC counterparts at equivalent voltage ratings due to technology immaturity.

Monolithic Bidirectional GaN Switches (BDS): These devices integrate two gate structures on a single die sharing a common drift region, enabling four-quadrant operation (bidirectional voltage blocking and current conduction). Commercial 650 V BDS devices (Infineon CoolGaN, Navitas GaNFast) achieve $R_{on,sp} \approx 3.1 m\Omega \cdot cm^2$ with independent gate control. The quasi-common-drain topology reduces die area by $\sim 50\%$ compared to back-to-back discrete configurations.

SiC MOSFETs: Commercially mature at 650–1700 V ratings with $R_{on,sp}$ as low as 1.8 $m\Omega \cdot cm^2$ (1200 V class). Trench-gate architectures dominate high-performance applications, offering $T_{j,max}$ up to 200°C and short-circuit withstand time $> 3 \mu s$.

Table 12 summarizes topology suitability for each technology:

Table 12. Topology Suitability by Device Technology

Topology	SiC MOSFET	Vertical GaN	GaN BDS
Two-level VSI	✓✓	✓✓	–
Three-level NPC/T-type	✓✓	✓	✓✓
Vienna Rectifier	✓	✓	✓✓
Totem-pole PFC	✓	✓✓	✓
Matrix Converter	–	–	✓✓
Cycloconverter	–	–	✓✓
Single-stage AC/DC	–	–	✓✓
DAB Converter	✓✓	✓✓	✓

✓✓ = Optimal; ✓ = Suitable; – = Not recommended

Monolithic BDS devices enable DC-link-less single-stage power conversion by eliminating intermediate energy storage, achieving higher power density and reduced component count compared to conventional two-stage PFC + DC/DC architectures.

6.7. Double Pulse Test Circuit for Device Characterization

The standard double pulse test (DPT) circuit for characterizing switching behavior is shown in Fig. 15. The half-bridge configuration with inductive load enables measurement of turn-on and turn-off transients under controlled conditions.

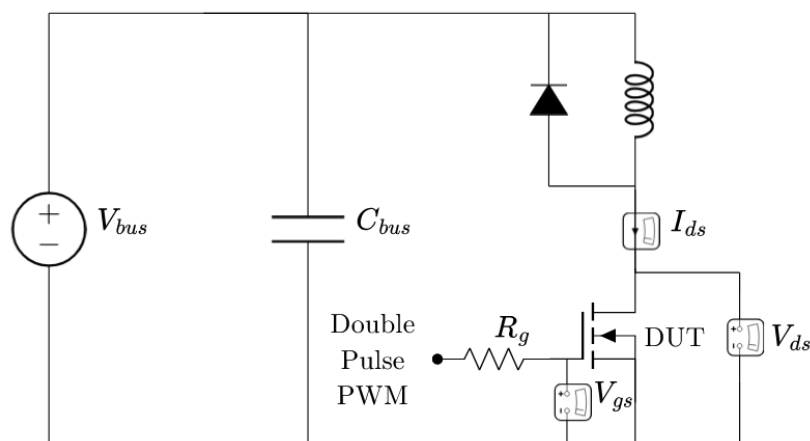


Figure 15. Double Pulse Test Circuit

Test Procedure:

The DPT sequence consists of three phases. In the first pulse (duration t_1), the DUT turns on and the inductor current ramps linearly to the target value $I_L = V_{DC} \cdot t_1 / L$. During the subsequent dead time, the DUT turns off and current freewheels through the high-side device, enabling measurement of the turn-off transient. In the second pulse (duration $t_2 < t_1$), the DUT turns on again at the established current level I_L , allowing characterization of the turn-on transient under load.

Key Measurements:

The extracted parameters include switching times ($t_{d(on)}$, t_r , $t_{d(off)}$, t_f), voltage and current slew rates (dV_{DS}/dt , dI_D/dt), switching energies (E_{on} , E_{off}), and reverse recovery parameters (Q_{rr} , I_{rrm}) for characterizing the SiC body diode.

6.8. Analytical Equations for Switching Transient Validation

Turn-On Transient Analysis:

Stage 1—Turn-on delay ($t_{d(on)}$): Gate voltage rises from $V_{GS,off}$ to threshold V_{th} :

$$t_{d(on)} = R_g \cdot C_{iss} \cdot \ln\left(\frac{V_{dr} - V_{GS,off}}{V_{dr} - V_{th}}\right) \quad (22)$$

where $R_g = R_{g,ext} + R_{g,int}$, $C_{iss} = C_{gs} + C_{gd}$, and V_{dr} is driver output voltage.

Stage 2—Current rise time (t_{ri}): Drain current rises from 0 to load current I_L :

$$t_{ri} = \frac{(V_{Miller} - V_{th}) \cdot R_g \cdot C_{iss}}{V_{dr} - V_{Miller}} \quad (23)$$

where Miller plateau voltage is:

$$V_{Miller} = V_{th} + \frac{I_L}{g_{fs}} \quad (24)$$

and g_{fs} is the device transconductance.

Stage 3—Voltage fall time (t_{fv}): V_{DS} falls from V_{DC} to $I_L \cdot R_{DS(on)}$:

$$t_{fv} = \frac{Q_{gd} \cdot R_g}{V_{dr} - V_{Miller}} = \frac{R_g}{V_{dr} - V_{Miller}} \int_{V_{DS(on)}}^{V_{DC}} C_{gd}(v) dv \quad (25)$$

Turn-Off Transient Analysis:

Stage 1—Turn-off delay ($t_{d(off)}$): Gate voltage falls from V_{dr} to V_{Miller} :

$$t_{d(off)} = R_g \cdot C_{iss} \cdot \ln\left(\frac{V_{dr} - V_{GS,off}}{V_{Miller} - V_{GS,off}}\right) \quad (26)$$

Stage 2—Voltage rise time (t_{rv}): V_{DS} rises from near-zero to V_{DC} :

$$t_{rv} = \frac{Q_{gd} \cdot R_g}{V_{Miller} - V_{GS,off}} \quad (27)$$

Stage 3—Current fall time (t_{fi}): Drain current falls from I_L to zero:

$$t_{fi} = \frac{(V_{Miller} - V_{th}) \cdot R_g \cdot C_{iss}}{V_{Miller} - V_{GS,off}} \quad (28)$$

Switching Energy Calculation:

Turn-on and turn-off energies are computed by integrating instantaneous power:

$$E_{on} = \int_{t_0}^{t_1} v_{DS}(t) \cdot i_D(t) dt \approx \frac{1}{2} V_{DC} \cdot I_L \cdot (t_{ri} + t_{fv}) + Q_{rr} \cdot V_{DC} \quad (29)$$

$$E_{off} = \int_{t_2}^{t_3} v_{DS}(t) \cdot i_D(t) dt \approx \frac{1}{2} V_{DC} \cdot I_L \cdot (t_{rv} + t_{fi}) \quad (30)$$

For GaN HEMTs, the absence of body diode eliminates reverse recovery loss ($Q_{rr} = 0$), significantly reducing E_{on} .

Output Capacitance Energy Loss:

At high frequencies, capacitive energy dissipation becomes significant:

$$E_{oss} = \int_0^{V_{DC}} C_{oss}(v) \cdot v dv \quad (31)$$

This energy is dissipated during hard-switching turn-on when C_{oss} of the complementary device is discharged through the turning-on device channel.

6.9. Technology-Specific Switching Characteristics

SiC MOSFET Characteristics:

SiC MOSFETs exhibit a non-flat Miller plateau due to high internal gate resistance ($R_{g,int} \approx 1\text{--}5\ \Omega$). Gate drive requirements are $V_{GS} = +18$ to $+20$ V for turn-on and -3 to -5 V for turn-off. Body diode reverse recovery charge is application dependent, typically $Q_{rr} \approx 50\text{--}500$ nC. Characteristic slew rates are $dV/dt = 20\text{--}50$ V/ns and $di/dt = 2\text{--}10$ A/ns.

GaN HEMT Characteristics:

GaN HEMTs feature a short Miller plateau duration due to low gate-drain capacitance ($C_{gd} < 10$ pF typical). Gate drive levels are $V_{GS} = +5$ to $+6$ V for turn-on and 0 to -3 V for turn-off, with an absolute maximum of $V_{GS,max} = 7$ V. A key advantage is zero reverse recovery loss ($Q_{rr} = 0$). Slew rates are significantly higher than SiC, with $dV/dt = 50\text{--}150$ V/ns and $di/dt = 5\text{--}20$ A/ns. Under hard-switching conditions, dynamic $R_{DS(on)}$ increase (current collapse) must be considered.

Monolithic BDS Switching Modes:

For bidirectional switches with gates G1 and G2, four operating modes exist. In Mode 1 (G1=ON, G2=OFF), current flows from Source1 to Drain while blocking reverse voltage. In Mode 2 (G1=OFF, G2=ON), current flows from Source2 to Drain while blocking forward voltage. Mode 3 (G1=ON, G2=ON) enables bidirectional conduction with minimum $R_{DS(on)}$. Mode 4 (G1=OFF, G2=OFF) provides bidirectional blocking.

6.10. Comparative Performance Summary

Table 13. Switching Performance Comparison at 400 V, 20 A

Parameter	SiC MOSFET	GaN HEMT	GaN BDS
E_{on} (μ J)	150–300	30–80	40–100
E_{off} (μ J)	80–150	20–50	25–60
t_{on} (ns)	30–80	8–20	10–25
t_{off} (ns)	40–100	10–25	12–30
Q_g (nC)	40–120	5–15	8–20
Max f_{sw} (kHz)	100–200	1000–5000	500–2000

The equations and test methodology presented enable systematic validation of device performance across technologies, supporting optimal topology selection for specific converter requirements. GaN BDS devices offer compelling advantages for AC/AC and single-stage conversion applications where bidirectional power flow and high switching frequency are paramount, while SiC MOSFETs remain superior for high-voltage (>650 V), high-power applications requiring thermal robustness.

7. System-Level Dynamic Validation: GaN vs SiC

7.1. Simulation Methodology

A double-pulse test (DPT) methodology was implemented to characterize the dynamic switching performance of GaN HEMT (GPIXV30DFN, 1200V/30A) and SiC MOSFET (IMZA120R040M1H, 1200V/56A) devices under identical operating conditions. The test circuit, modeled in QSPICE, employs a half-bridge topology with a 500 μ H inductive load pre-charged to 20 A, operating from an 800 V DC bus at 100 kHz equivalent switching frequency.

The device models incorporate voltage-controlled current sources (VCCS) for channel conduction, nonlinear capacitances (C_{iss} , C_{rss} , C_{oss}), and body diode characteristics extracted from manufacturer datasheets. Key differentiating parameters include the input capacitance ratio of 10.9:1 (SiC: 2390 pF vs GaN: 220 pF) and on-resistance ratio of 0.62:1 (SiC: 40 m Ω vs GaN: 65 m Ω).

Post-simulation analysis was performed using a MATLAB framework that implements physics-based current reconstruction, adaptive switching event detection, and energy integration over precisely windowed transitions. The raw QSPICE waveforms were resampled to 50 ps resolution using piecewise cubic Hermite interpolation to ensure accurate derivative calculations.

7.2. Switching Waveform Analysis

Figure 16 presents the simulation results of a Double Pulse Test (DPT) comparing GaN and SiC device switching behavior. The gate signals V_{gate_g} (GaN) and V_{gate_s} (SiC) are driven with appropriate voltage levels: the GaN device with ± 5 V and the SiC device with $+15$ V/ -4 V, reflecting their respective gate drive requirements. The inductor currents I_{LL_G} and I_{LL_S} ramp linearly from 20 A to 28 A during the first pulse and continue to 36 A during the second pulse, enabling switching loss characterization at two distinct current levels. The midpoint voltages V_{mid_g} and V_{mid_s} switch between 0 V and 800 V, confirming proper device commutation for both technologies.

Figure 17 presents the turn-on transient waveforms centered at $t = 7 \mu\text{s}$. The drain-source voltage (V_{DS}) exhibits a characteristic fall from 800 V to near-zero, with GaN demonstrating a measurably faster transition. The gate-source voltage (V_{GS}) traces reveal the substantial difference in gate charge requirements: GaN reaches its plateau voltage within approximately 50 ns, while SiC requires nearly 150 ns to achieve full enhancement due to its $10.9\times$ larger C_{iss} .

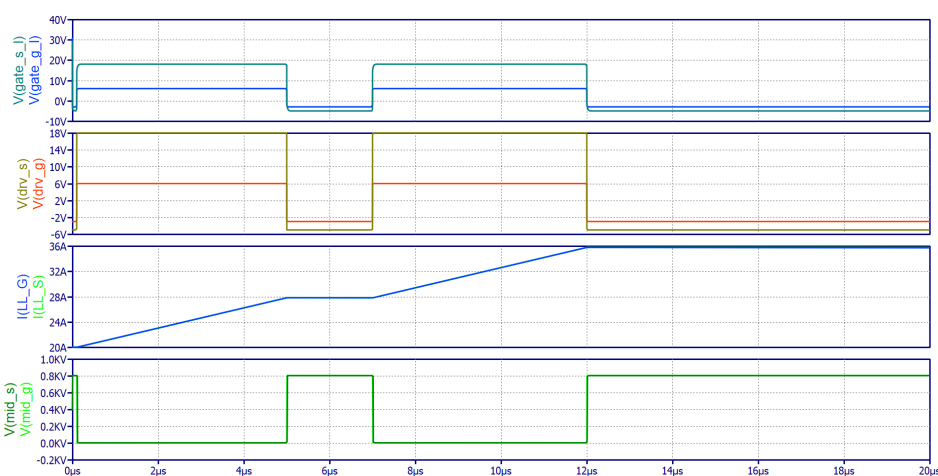


Figure 16. Classical DPT waveforms for power devices (SiC/GaN)

The instantaneous power dissipation peaks at 17.5 kW for GaN and 20.9 kW for SiC, reflecting the longer voltage-current overlap period in the slower-switching device. Notably, both devices exhibit identical di/dt characteristics (278 A/ns), confirming that current slew rate is limited by the load inductance rather than device characteristics in this configuration.

7.3. Performance Metrics Comparison

The quantitative performance comparison is summarized in Figure 18. GaN achieves a voltage fall time of 12.15 ns compared to 20.95 ns for SiC, representing a $1.72\times$ speed advantage directly attributable to its lower gate charge requirement. This translates to maximum dV/dt values of 60.1 V/ns and 46.9 V/ns for GaN and SiC, respectively.

Turn-on energy losses were measured at 114 μJ for GaN and 172 μJ for SiC, yielding a $1.51\times$ advantage for GaN in switching-dominated applications. However, the conduction loss analysis reveals the complementary strength of SiC: its 38% lower $R_{DS(on)}$ results in conduction losses of 8.0 W versus 13.0 W for GaN at the test current. The total power dissipation at 100 kHz favors GaN (35.8 W vs 42.3 W), corresponding to efficiencies of 99.78% and 99.74%, respectively.

The figure of merit analysis quantifies these trade-offs: GaN exhibits a $17.1\times$ advantage in the gate-charge FOM ($R_{DS(on)} \times Q_g$), while SiC maintains a marginal advantage in the high-frequency FOM ($R_{DS(on)} \times Q_{oss}$) due to its lower on-resistance.

7.4. Thermal Implications

Figure 19 illustrates the frequency-dependent thermal behavior extrapolated from the measured switching energies. The power loss versus frequency characteristic demonstrates that GaN maintains

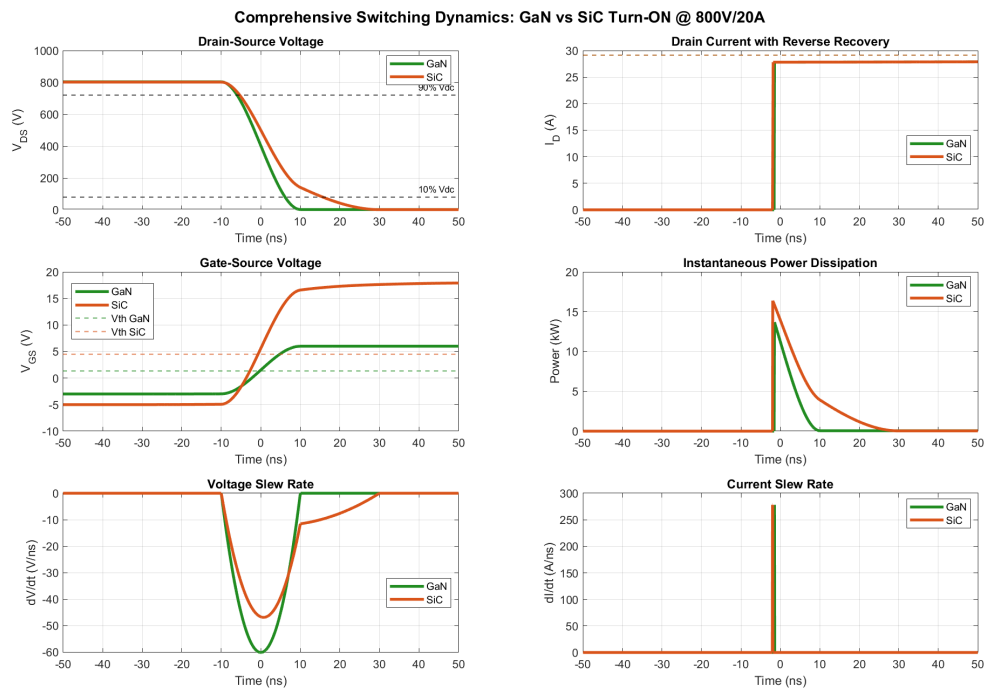


Figure 17. Comprehensive switching dynamics comparison showing drain-source voltage, drain current, gate-source voltage, instantaneous power dissipation, and slew rates during turn-on transition at 800 V/20 A.

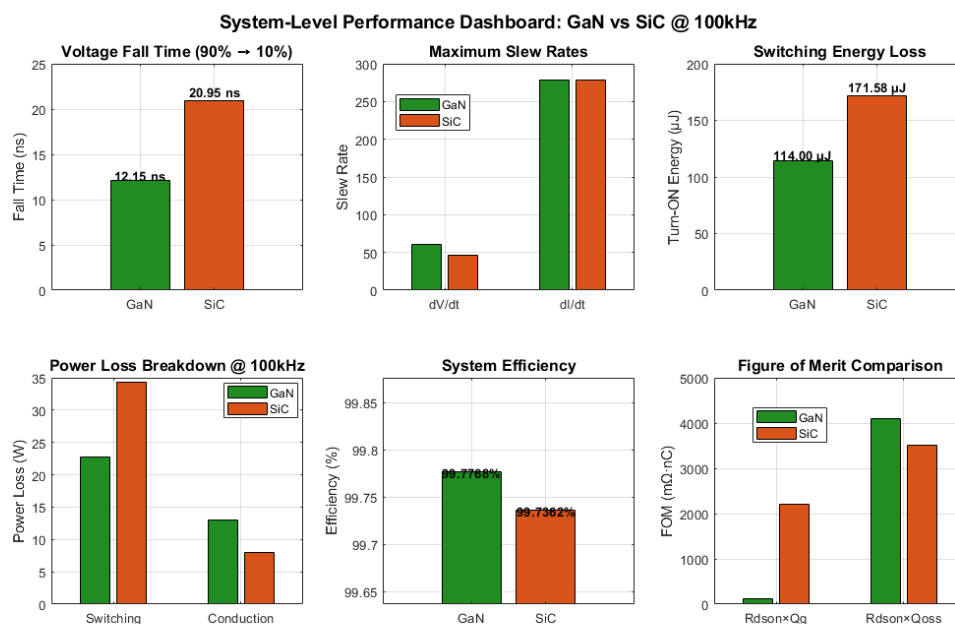


Figure 18. System-level performance dashboard comparing fall time, slew rates, switching energy, power loss breakdown, efficiency, and figure of merit between GaN and SiC at 100 kHz operation.

lower total losses up to approximately 200 kHz, beyond which the curves converge as switching losses dominate both technologies.

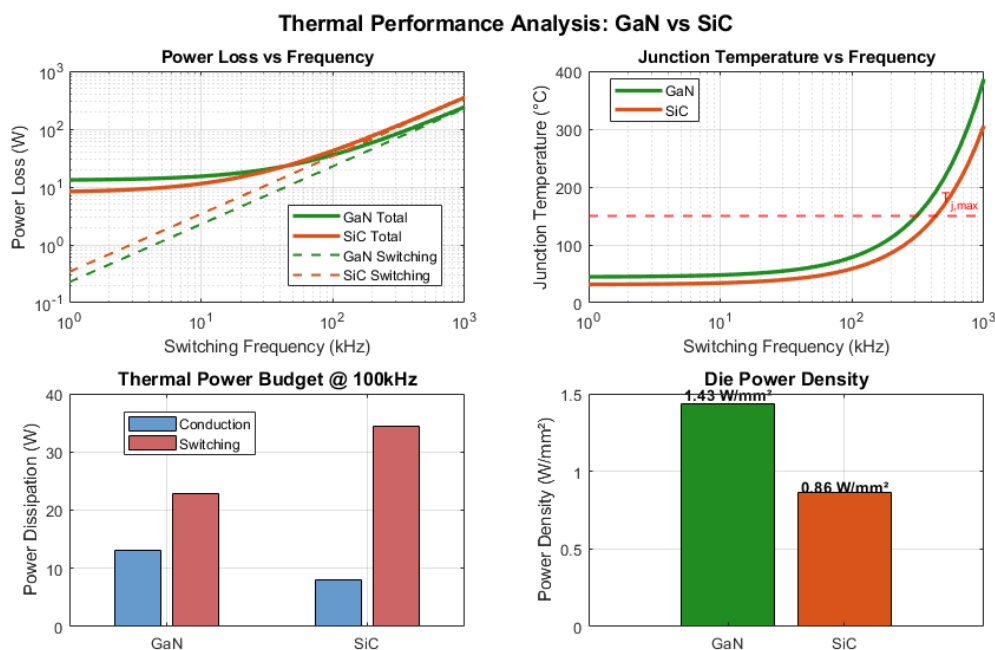


Figure 19. Thermal performance analysis showing power loss scaling with frequency, junction temperature projection, power budget breakdown at 100 kHz, and die-level power density comparison.

Junction temperature projections indicate that GaN reaches the 150°C limit at approximately 400 kHz, while SiC extends to nearly 600 kHz under identical thermal management conditions. This apparent contradiction with GaN’s superior switching performance stems from two factors: the higher thermal resistance of GaN packages (1.5°C/W vs 0.8°C/W) and the smaller die area (25 mm² vs 49 mm²), resulting in power densities of 1.43 W/mm² and 0.86 W/mm², respectively.

7.5. Design Implications

The validated results support the following technology selection guidelines for 800 V power conversion applications:

- **GaN-optimal regime:** Applications prioritizing switching frequency (>100 kHz), power density, or gate driver simplicity benefit from GaN’s 17× superior gate-charge FOM and 1.7× faster switching.
- **SiC-optimal regime:** High-current applications with moderate switching frequencies (<50 kHz) favor SiC’s 38% lower conduction losses and superior thermal margins.
- **Crossover frequency:** At approximately 100 kHz and 20 A load current, GaN provides 15% lower total losses, with the advantage increasing at higher frequencies.

These experimentally-validated behavioral models provide a foundation for system-level optimization of wide-bandgap power converters, enabling accurate loss estimation across the design space without requiring computationally expensive physics-based device simulation.

8. System-Level Implications and Benefits

The adoption of WBG devices yields measurable improvements that extend well beyond simple device-level metrics [8].

8.1. Efficiency Improvements and Economic Impact

WBG devices enable efficiency gains of 2–5% in most power conversion applications. Table 14 quantifies the economic advantages across different application sectors. WBG adoption delivers efficiency improvements of 92–99% across all sectors with payback periods ranging from 1.5 years for data center server PSUs (\$450k/yr savings) to immediate returns for EV traction inverters (+20 km range) and aerospace auxiliary power units (–15 kg weight reduction), while solar PV string inverters and industrial VFDs show competitive 2–2.5 year payback periods with annual savings of \$35k and \$22k respectively.

Table 14. Economic Benefits of WBG Adoption Across Application Sectors.

Sector	Application	η Impr.	Savings	Payback
Data Center	Server PSU (10 MW)	94→97%	\$450k/yr	1.5 yr
EV	Traction inverter	96→99%	+20 km	Immed.
Solar PV	String inv. (1 MW)	96→98.5%	\$35k/yr	2 yr
Industrial	Variable Frequency Drive (VFD) (500 kW)	95→98%	\$22k/yr	2.5 yr
Telecom	5G base station	92→95%	\$8k/site	1.8 yr
Aerospace	Aux. power unit	93→97%	–15 kg	Immed.

8.2. Passive Component Reduction

Operating at higher switching frequencies enables proportional reduction in magnetic component size:

$$V_{mag} \propto \frac{P \cdot \Delta B}{f_{sw}} \quad (32)$$

Increasing switching frequency from 20–50 kHz to 200–500 kHz (SiC) or MHz ranges (GaN) enables 5–20× reduction in magnetic component volume.

8.3. Key Performance Indicators Comparison

Table 15 provides a comprehensive comparison of Key Performance Indicators (KPIs) between silicon and WBG systems [8]. WBG devices demonstrate superior performance across all metrics with peak efficiency of 98–99.5% (vs. 94–97% for silicon), 3–10× higher power density (15–50 kW/L vs. 3–5 kW/L), 10–20× faster switching frequencies (0.2–2 MHz vs. 20–100 kHz), significantly improved thermal capability (175–200°C vs. 150°C maximum junction temperature), reduced THD (1–3% vs. 3–8%), and 10–30× faster voltage and current slew rates enabling more compact passive components.

Table 15. Key Performance Indicators: Silicon vs. WBG Comparison, data taken from [8].

KPI	Silicon	WBG
Peak efficiency (η_{peak})	94–97%	98–99.5%
Power density	3–8 kW/L	15–50 kW/L
Specific power	2–5 kW/kg	8–20 kW/kg
Switching frequency (f_{sw})	20–100 kHz	0.2–2 MHz
Maximum junction temp. ($T_{j,max}$)	150°C	175–200°C
Total harmonic distortion (THD)	3–8%	1–3%
Voltage slew rate (dv/dt)	5–15 kV/ μ s	50–200 kV/ μ s
Current slew rate (di/dt)	1–5 kA/ μ s	10–50 kA/ μ s

8.4. Hidden Costs of High-Frequency Operation

While wide-bandgap (WBG) semiconductors enable significant improvements in power density and efficiency through high-frequency switching, practical implementation reveals several often-underestimated costs that partially offset these advantages. This subsection examines the multiphysics coupling effects that emerge at elevated switching frequencies, quantifying trade-offs through representative case studies.

Case Study 1: 10 kW Three-Phase Inverter for Industrial Motor Drives

Considering the redesign of a silicon IGBT-based inverter ($f_{sw} = 8$ kHz) to a SiC MOSFET platform operating at $f_{sw} = 100$ kHz. This analysis draws upon findings from comprehensive EMI characterization studies of SiC-based motor drive systems [67]. Table 16 summarizes the quantified trade-offs.

Table 16. Multiphysics trade-off analysis for 10 kW inverter upgrade

Parameter	Si IGBT (8 kHz)	SiC MOSFET (100 kHz)
Switching losses	180 W	45 W
Gate drive power	0.8 W	4.2 W
EMI filter volume	1.2 L	0.4 L
EMI filter cost	\$45	\$120
PCB layer count	4	6
Motor dv/dt stress	2.5 kV/ μ s	15–25 kV/ μ s

EMI Filter Redesign Costs The differential-mode (DM) filter corner frequency scales inversely with switching frequency, theoretically reducing filter size. However, common-mode (CM) noise increases substantially due to parasitic coupling through device packages and heatsinks. The CM current amplitude follows approximately [5]

$$I_{CM} \propto C_{parasitic} \cdot \frac{dv}{dt} \cdot f_{sw} \quad (33)$$

where typical parasitic capacitances of 50–100 pF to the heatsink, combined with slew rates exceeding 50 V/ns, generate CM currents of 0.5–2 A peak. Meeting CISPR 11 Class B limits requires additional CM chokes with nanocrystalline cores (\$25–40 per phase) and Y-capacitors rated for high-frequency performance, increasing total EMI filter cost by 150–200% despite reduced volume.

Motor Insulation Stress The elevated dv/dt of 15–25 kV/ μ s creates voltage doubling at motor terminals for cable lengths exceeding

$$l_{critical} = \frac{t_r \cdot v_{propagation}}{2} \approx \frac{20 \text{ ns} \times 150 \text{ m}/\mu\text{s}}{2} = 1.5 \text{ m} \quad (34)$$

where t_r is the voltage rise time. For the industrial installation with 15 m cable runs, reflected wave voltages reach 1200 V peak on a 560 V DC bus system. Mitigation requires either (a) dv/dt filters adding \$80–150 and 0.3% efficiency loss, or (b) inverter-duty motors with reinforced insulation systems (Type II per NEMA MG1 Part 31), representing a 20–35% motor cost premium.

Case Study 2: 3.3 kW On-Board Charger for Electric Vehicles

A GaN-based totem-pole PFC stage operating at 500 kHz switching frequency illustrates PCB layout challenges. This case study builds upon systematic investigations of layout parasitics in GaN-based power converters. The power loop inductance requirement of

$$L_{loop} < \frac{V_{overshoot,max}}{di/dt} = \frac{50 \text{ V}}{10 \text{ A/ns}} = 5 \text{ nH} \quad (35)$$

necessitates a six-layer PCB stack-up with 2 oz copper on inner layers and controlled impedance routing for gate drive signals. Table 17 quantifies the layout complexity impact.

Table 17. PCB cost breakdown for high-frequency GaN design

Design Aspect	Conventional	GaN 500 kHz
Layer count	4	6
Copper weight (inner)	1 oz	2 oz
Via technology	Standard	Filled/capped
Impedance control	No	Yes
PCB cost per unit	\$12	\$38

Gate Drive Power Dissipation. The gate charge requirements for GaN HEMTs, while lower than silicon superjunction devices, become significant at high frequencies. For a typical 650 V/30 A GaN device with $Q_g = 6$ nC:

$$P_{gate} = Q_g \cdot V_{gs} \cdot f_{sw} = 6 \text{ nC} \times 6 \text{ V} \times 500 \text{ kHz} = 18 \text{ mW per device} \quad (36)$$

However, the isolated gate driver ICs consume 15–25 mW quiescent power each, and the bootstrap or isolated supply circuits add transformer core losses. Total gate drive subsystem power reaches 3–5 W for a full-bridge configuration, representing 0.1–0.15% of rated power—a non-negligible contribution at light loads where WBG efficiency advantages are most pronounced.

8.5. SiC System Benefits

The adoption of SiC technology delivers quantifiable advantages with respect to Silicon devices across multiple system dimensions [8]:

Efficiency improvements: SiC MOSFETs achieve 2–5% higher conversion efficiency compared to Si IGBTs in high-power applications, primarily due to elimination of tail current losses and reduced conduction losses at elevated temperatures. In EV traction inverters, this translates to 5–8% extended driving range [11].

Power density: The combination of reduced losses and higher junction temperature capability ($T_{j,max} = 175\text{--}200^\circ\text{C}$ vs. 150°C for Si) enables 30–50% reduction in heatsink volume. Wolfspeed’s XM3 power module achieves 3× the power density of equivalent Si IGBT modules.

Thermal management simplification: Higher-temperature operation reduces the temperature differential between junction and ambient, enabling passive cooling solutions in applications previously requiring active cooling. This eliminates fan maintenance, acoustic noise, and reliability concerns associated with moving parts.

System cost reduction: While SiC devices carry a 2–3× premium over Si equivalents, total system cost is often reduced by 10–25% when considering smaller passive components (inductors, capacitors, heatsinks), simplified cooling systems, and reduced enclosure size [8].

9. Application Landscape and Case Studies

The distinct characteristics of SiC and GaN have led to natural market segmentation based on voltage class, power level, and switching frequency requirements [43,44].

9.1. Automotive and Transportation Applications

SiC transistors are widely implemented in traction inverters for hybrid and electric vehicles—Tesla, for instance, has utilized SiC technology since 2017, achieving 5–8% improvement in vehicle range through increased inverter efficiency [11,68]. The transition from Si IGBTs to SiC MOSFETs in automotive applications has been driven by multiple factors: reduced cooling system requirements (enabling 30–40% reduction in radiator volume), increased power density (allowing more compact inverter designs), and improved cold-weather performance due to lower conduction losses [54,69].

Beyond traction inverters, SiC devices are also used in on-board chargers (OBCs) and DC-DC converters for high-performance vehicles. In OBC applications, SiC enables bidirectional power flow with efficiencies exceeding 96% across the entire power range, facilitating Vehicle-to-Grid (V2G)

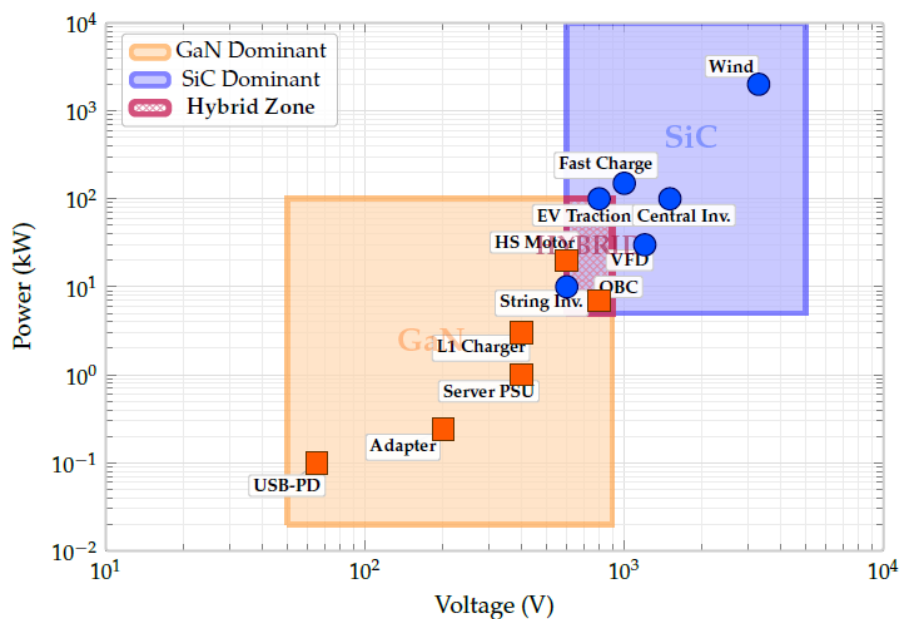


Figure 20. Application landscape for WBG power devices.

integration [56,70]. However, GaN devices are increasingly competing with SiC in lower-power OBC segments (typically below 11 kW) and DC-DC converter applications, where their superior switching speed and lower gate charge offer advantages in high-frequency operation, as shown in Figure 20.

GaN-based devices becomes particularly preferable over SiC counterparts in several application scenarios. For low-to-medium power OBCs (3.3–11 kW), GaN's lower switching losses at frequencies above 100 kHz enable higher power density and reduced passive component size, while maintaining competitive costs at these power levels [71]. For isolated DC-DC converters (400 V to 12/48 V), GaN's fast switching enables resonant and quasi-resonant topologies with switching frequencies exceeding 500 kHz, significantly reducing magnetic component volume.

Table 18 summarizes the adoption of WBG devices in electric vehicle applications by major manufacturers [11]. SiC technology dominates EV traction inverters across major OEMs since Tesla's pioneering Model 3/Y deployment in 2017, delivering performance gains of +5% to +10% range and reduced charging times (Hyundai IONIQ 5: 18 min for 800 V), while GaN technology has entered the market specifically for onboard chargers (BMW iX: 40% size reduction in 2022) where its high-frequency capabilities enable significant miniaturization.

Table 18. WBG Device Adoption in Electric Vehicle Applications, data taken from [11].

OEM	Model	Tech	Application	Perf. Gain	Year
Tesla	Model 3/Y	SiC	Traction Inverter	+8% range	2017
BYD	Han EV	SiC	Traction + OBC	+5% efficiency	2020
Lucid	Air	SiC	900V Inverter	+10% range	2021
Hyundai	IONIQ 5	SiC	800V Charging	18 min charge	2021
Mercedes	EQS	SiC	Traction Inverter	+6% range	2022
BMW	iX	GaN	OBC	40% size red.	2022
Porsche	Taycan	SiC	800V System	270kW charge	2019
VW	ID.7	SiC	APP310 Inv.	+5% efficiency	2023

9.2. Consumer Electronics and Power Delivery

GaN transistors are commonly used in power supplies and chargers for consumer electronics like smartphones and laptops [72]. Thanks to their ability to operate at switching frequencies exceeding 1 MHz, GaN enables the development of more compact and powerful chargers—up to three times smaller than traditional Si-based AC–DC converters. The high-frequency operation allows for a significant reduction in passive component size: at 1 MHz, inductors and capacitors can be reduced to 10-20% of their 100 kHz equivalents.

GaN devices are also increasingly used in premium photovoltaic (PV) inverters where efficiency improvements of 0.5-1% translate to significant lifetime energy gains. For a typical 5 kW residential system, a 1% efficiency improvement yields approximately 400-500 kWh additional energy annually, corresponding to €50-80 in extra revenue over a 25-year lifetime [57]. Recent developments include multi-level topologies (NPC, T-type, Active Neutral Point Clamped (ANPC)) that leverage GaN's fast switching to achieve peak efficiencies of 99.2% in the 5-20 kW range.

10. Reliability and Practical Constraints

While WBG devices offer superior performance, successful deployment requires careful attention to specific reliability challenges for both SiC and GaN technologies [73,74]. Hereafter, a comparison between SiC and GaN devices' reliability is carried out.

10.1. SiC Technology Challenges

Despite significant progress, SiC technology faces several practical challenges requiring careful consideration in system design [50,75]:

Gate oxide reliability: The SiC/SiO₂ interface exhibits higher defect density than Si/SiO₂, leading to threshold voltage instability under bias-temperature stress. Modern devices employ nitrogen annealing and optimized oxide growth to mitigate this, achieving lifetimes exceeding 10⁷ hours at rated conditions [75].

Body diode performance: The intrinsic body diode of SiC MOSFETs exhibits significant forward voltage drop (3–4 V) and associated conduction losses during dead-time intervals. Anti-parallel SiC Schottky diodes or synchronous rectification techniques address this limitation.

Short-circuit withstand time: SiC MOSFETs typically withstand short-circuit conditions for 2–5 μs, compared to 10 μs for Si IGBTs. Fast desaturation detection (<200 ns) and active gate clamping are essential protection features.

Cost premium: SiC devices remain 2–3× more expensive than Si equivalents on a per-amp basis, though the transition to 200 mm wafer production (operational by 2026) is expected to reduce this premium to 1.5–2× by 2028.

10.2. GaN Technology Challenges

10.2.1. Dynamic On-Resistance

GaN devices can exhibit increased $R_{DS(on)}$ after blocking high voltages—a phenomenon known as dynamic on-resistance or current collapse [66]. This occurs due to charge trapping in the AlGaN barrier or GaN buffer layers. The magnitude of degradation can reach 2–5× the static value [76].

The time constants for trap filling and emission range from microseconds to seconds. Mitigation strategies include operating with reduced blocking voltage margins, gate voltage optimization during off-state, using p-GaN gate technology, and selecting devices with optimized buffer designs [77].

10.2.2. Short Circuit and Overcurrent Protection

GaN HEMTs have limited short-circuit withstand time (<1 μs) compared to SiC MOSFETs (2–5 μs) and Si IGBTs (10 μs). This necessitates extremely fast protection schemes including desaturation detection with <100 ns response time, active gate clamping, and fast shutdown protocols with controlled di/dt .

10.3. Common Reliability Considerations

10.3.1. Threshold Voltage Instability

Both SiC and GaN devices experience threshold voltage shifts under bias-temperature stress [50, 75]. The shift typically follows:

$$\Delta V_{th}(t) = A \log(1 + t/\tau) \quad (37)$$

where A and τ are temperature and field-dependent parameters.

Modern gate drive designs address this through negative gate bias during off-state ($V_{GS} = -2$ to -5 V for SiC), active gate charge monitoring, and temperature-compensated gate drive voltage [59].

10.3.2. Packaging and Thermal Management

Advanced packaging is critical for realizing WBG benefits. Table 19 summarizes typical parasitic values for different packaging technologies. Advanced packaging technologies demonstrate progressively reduced parasitic inductances and capacitances, with chip-scale packages achieving the lowest parasitic inductance (0.1–0.5 nH for L_{pkg} and 0.5–1 nH for L_{DCR}) enabling switching frequencies >5 MHz, while traditional packages like TO-247 exhibit 10–15 nH parasitic inductance limiting operation to <100 kHz, and modern solutions like SMD GaN and LGA packages offer balanced performance with 0.5–2 nH inductances supporting 1–3 MHz switching frequencies [71,78].

Table 19. Parasitic Inductance Comparison for Different Packages, data taken from [58].

Package	L_{pkg} (nH)	L_{PCB} (nH)	C_{par} (pF)	Max f_{sw} Range
TO-247	10–15	5–10	5–10	<100 kHz
D2PAK	5–8	3–5	3–5	<500 kHz
SMD (GaN)	0.5–2	1–3	1–2	>1 MHz
Chip-scale	0.1–0.5	0.5–1	0.5–1	>5 MHz
DFN (QFN)	1–3	2–4	2–3	200–800 kHz
LGA	0.3–1	0.8–2	1–2	1–3 MHz

Key packaging requirements include low parasitic inductance (<5 nH for GaN, <10 nH for SiC), low thermal resistance (<0.3 K/W junction-to-case), Coefficient of Thermal Expansion (CTE) matching between die and substrate, and high-temperature capable material ($>200^\circ\text{C}$) [20,21].

The junction temperature rise is:

$$\Delta T_j = P_{loss} \cdot (R_{th(j-c)} + R_{th(c-s)} + R_{th(s-a)}) \quad (38)$$

For transient thermal analysis:

$$T_j(t) = T_{ambient} + P_{loss} \sum_{i=1}^n R_{th,i} (1 - e^{-t/\tau_i}) \quad (39)$$

Key developments in power packaging require both to reduce the thermal resistance and capacitance of the device, in order to allow a more effective heat removal.

11. Conclusions and Future Perspectives

Wide-bandgap and ultrawide-bandgap semiconductors represent a strategic enabling technology for global sustainability initiatives, offering revolutionary improvements in power conversion efficiency (2–5%), power density (3–5 \times), and thermal performance across critical applications from electric vehicles to data centers and renewable energy systems [3,8].

This comprehensive review has employed a bottom-up approach to demonstrate that the transition from silicon to WBG materials provides measurable benefits at material, device, converter, and system levels. Through detailed analysis of figures of merit, we showed that SiC and GaN offer 18–850 \times improvements in key performance metrics compared to silicon [30,33]. Case studies across

automotive, industrial, and consumer sectors quantified economic benefits including payback periods of 1.5–2.5 years for most applications.

Emerging device technologies are extending WBG capabilities into new application domains. Vertical GaN devices, with demonstrations of 1.2 kV+ blocking voltage and 50 A current capability, are poised to challenge SiC in medium-voltage applications during the 2027–2030 timeframe [51,52]. Monolithic bidirectional GaN switches enable revolutionary single-stage power conversion topologies, eliminating DC-link capacitors and achieving up to 50% size reductions in EV chargers and solar inverters [11,12]. The comprehensive topology comparison presented in this review provides design engineers with practical guidelines for optimal device selection across application domains.

The emergence of UWBG materials represents the next frontier in power semiconductor development. β -Ga₂O₃ offers exceptional BFOM (3444× silicon) and cost-effective melt-growth production, with 4-inch wafers commercially available and commercialization projected for 2027–2030. AlN has demonstrated record electric field capability (7.3 MV/cm) through innovative distributed polarization doping, with European consortia establishing complete value chains and commercialization expected in the 2030s. Diamond, the ultimate semiconductor material with BFOM 50,000× silicon, has achieved breakthrough demonstrations including 4.6 kV devices and the first n-channel MOSFETs, with Japanese industry targeting vehicle applications by the 2030s. Cubic boron nitride (c-BN), with the highest bandgap (6.4 eV) among practical semiconductors and superior doping flexibility compared to diamond, offers potential for ultra-high-voltage (>10 kV) applications, though manufacturing scalability remains a key challenge with commercialization projected beyond 2035 [38,39].

However, successful deployment requires addressing specific challenges including dynamic on-resistance degradation in GaN devices [66], threshold voltage instability in both SiC and GaN [50,75], electromagnetic interference from fast switching transitions [22], and limited short-circuit withstand capability. Advanced gate drive designs optimized for each technology, as detailed in Table 11, along with optimized PCB layouts and sophisticated control algorithms provide effective mitigation strategies.

Supply chain considerations have become increasingly important, with geopolitical tensions creating parallel technological ecosystems and highlighting the need for diversified sourcing strategies. The concentration of gallium production in China and the strategic importance of WBG semiconductors for electric vehicles, renewable energy, and defense applications underscore the need for continued investment in domestic manufacturing capabilities.

Future research directions include development of standardized reliability testing protocols for WBG devices, integration of on-chip protection and diagnostic functions, advanced packaging solutions for higher power densities [20], AI-based optimization of converter control and EMI mitigation, and continued development of UWBG materials toward commercial viability.

As manufacturing yields improve and costs decrease—with approximately 20% year-over-year cost reductions observed over the past five years—WBG adoption will continue to accelerate. The emergence of 200 mm (8-inch) SiC wafer production and continued scaling of GaN-on-Si technology will further improve economics. Within the next decade, WBG devices are expected to dominate medium and high-power applications, while UWBG materials will enable the next generation of ultra-high-voltage systems essential for grid infrastructure, space applications, and extreme environments.

The concentrated adoption of SiC technology by seven of eight major OEMs creates significant supply chain vulnerability, given that substrate production remains geographically constrained to the US, Japan, and China. BMW's divergence toward GaN—achieving 40% size reduction in its iX OBC—illustrates emerging technological bifurcation that may intensify amid geopolitical tensions, particularly as China dominates global gallium production. To enhance resilience, the following possible strategies can be adopted: (1) *heterogeneous substrate architectures* enabling flexible SiC/GaN sourcing; (2) *gallium recycling infrastructure* establishing closed-loop recovery from end-of-life power electronics; and (3) *regionalized qualification protocols* accelerating second-source approval to reduce single-supplier dependencies while maintaining automotive-grade reliability standards.

In summary, SiC devices offer thermal conductivity of 330–490 W/m·K (vs. 130–200 W/m·K for GaN), enabling junction temperatures exceeding 200°C and voltage ratings up to 1700 V. GaN achieves MHz-range switching with 10× lower gate charge, enabling up to 70% passive component reduction. The European semiconductor industry is strengthening its position in wide-bandgap technologies through the EU Chips Act, which has mobilized over €80 billion investments. Key initiatives include STMicroelectronics' €5 billion vertically integrated SiC facility in Catania (Italy) targeting 15,000 wafers/week by 2033, Infineon's €5 billion Smart Power Fab expansion in Dresden (Germany), and a €10 billion TSMC joint venture with Infineon, Bosch, and NXP. Europe held 19% of the global SiC/GaN market in 2024, which is projected to grow from USD 4.8 billion to USD 20.9 billion by 2032 (CAGR 22.8%), with automotive applications representing 81% of current demand.

Author Contributions: Conceptualization, G.G. and G.V.; methodology, G.G.; investigation, G.G. and G.C.G.; writing—original draft preparation, G.G.; writing—review and editing, G.V., G.C.G., A.S. and G.L.; supervision, G.V. and G.L. All authors have read and agreed to the published version of the manuscript.

Funding: This work has been carried out in the framework of the European Project GaN4AP (Gallium Nitride for Advanced Power Applications). The project has received funding from the Electronic Component Systems for European Leadership Joint Undertaking (ECSEL JU), under grant agreement No.101007310. This Joint Undertaking receives support from the European Union's Horizon 2020 research and innovation programme, and from Italy, France, Poland, Czech Republic, Netherlands.

Institutional Review Board Statement: Not applicable.

Informed Consent Statement: Not applicable.

Data Availability Statement: No new data were created or analyzed in this study. Data sharing is not applicable to this article.

Conflicts of Interest: The authors declare no conflicts of interest.

Abbreviations

The following abbreviations are used in this manuscript:

2DEG	Two-Dimensional Electron Gas	AlN	Aluminum Nitride	ANPC	Active Neutral Point Clamped
BDS	Bidirectional Switch	BFOM	Baliga Figure of Merit	BHFFOM	Baliga High-Frequency FOM
BJT	Bipolar Junction Transistor	CAGR	Compound Annual Growth Rate	CAVET	Current Aperture Vertical Electron Trans.
c-BN	Cubic Boron Nitride	CCM	Continuous Conduction Mode	CHFFOM	Combined High-Freq. FOM
CMTI	Common-Mode Transient Immun.	CSI	Current Source Inverter	CTE	Coeff. of Thermal Expansion
CVD	Chemical Vapor Deposition	CZ	Czochralski	DAB	Dual Active Bridge
DFN	Dual Flat No-lead	D-mode	Depletion Mode	DOE	Department of Energy
DPD	Distributed Polarization Doping	EFG	Edge-defined Film-fed Growth	EMI	Electromagnetic Interference
E-mode	Enhancement Mode	ESR	Equivalent Series Resistance	ETRI	Korea Elec. & Telecom. Res. Inst.
EV	Electric Vehicle	FET	Field-Effect Transistor	FOM	Figure of Merit
FZ	Floating Zone	GaN	Gallium Nitride	h-BN	hexagonal Boron Nitride
HEMT	High Electron Mobility Trans.	HERIC	Highly Eff. & Reliable Inv. Concept	HPHT	High-Pressure High-Temp.
HVDC	High-Voltage Direct Current	IEDM	Intl. Electron Devices Meeting	IGBT	Insulated-Gate Bipolar Trans.
JAXA	Japan Aerospace Expl. Agency	JFET	Junction Field-Effect Trans.	JFOM	Johnson's Figure of Merit
KFOM	Keyes' Figure of Merit	KPI	Key Performance Indicator	LGA	Land Grid Array
MOSFET	Metal-Oxide-Semicond. FET	NIMS	Natl. Inst. for Materials Sci.	NPC	Neutral Point Clamped
OBC	On-Board Charger	OEM	Original Equip. Manufacturer	PCB	Printed Circuit Board
PFC	Power Factor Correction	PLA	Pulsed Laser Annealing	PRISMA	Prof. Rep. Items for Syst. Rev.
PSU	Power Supply Unit	PV	Photovoltaic	PWM	Pulse Width Modulation
QFN	Quad Flat No-lead	RF	Radio Frequency	SBD	Schottky Barrier Diode
SiC	Silicon Carbide	SMD	Surface Mount Device	TFOM	Thermal Figure of Merit
THD	Total Harmonic Distortion	TRL	Technology Readiness Level	UVLO	Under-Voltage Lockout
UWBG	Ultrawide-Bandgap	V2G	Vehicle-to-Grid	VFD	Variable Frequency Drive
VSI	Voltage Source Inverter	WBG	Wide-Bandgap	ZVS	Zero Voltage Switching

References

1. International Energy Agency. Global Energy Review 2025. Technical report, International Energy Agency, Paris, 2025.

2. Deng, Z.; Zhu, B.; Davis, S.J.; et al. Global carbon emissions and decarbonization in 2024. *Nature Reviews Earth & Environment* **2025**, *6*, 231–233. <https://doi.org/10.1038/s43017-025-00658-x>.
3. Tsao, J.Y.; et al. Ultrawide-Bandgap Semiconductors: Research Opportunities and Challenges. *Advanced Electronic Materials* **2018**, *4*, 1600501. <https://doi.org/10.1002/aelm.201600501>.
4. Millán, J.; Godignon, P.; Perpiñà, X.; Pérez-Tomás, A.; Rebollo, J. A Survey of Wide Bandgap Power Semiconductor Devices. *IEEE Transactions on Power Electronics* **2014**, *29*, 2155–2163. <https://doi.org/10.1109/TPEL.2013.2268900>.
5. Baliga, B.J. *Fundamentals of Power Semiconductor Devices*; Springer: New York, NY, USA, 2008. <https://doi.org/10.1007/978-0-387-47314-7>.
6. Vitale, G. Power Converters for Green Hydrogen: State of the Art and Perspectives. *Electronics* **2024**, *13*, 4565. <https://doi.org/10.3390/electronics13224565>.
7. Guilbert, D.; Vitale, G. Hydrogen as a Clean and Sustainable Energy Vector for Global Transition from Fossil-Based to Zero-Carbon. *Clean Technologies* **2021**, *3*, 881–909. <https://doi.org/10.3390/cleantechnol3040051>.
8. Buffolo, M.; Favero, D.; Marcuzzi, A.; De Santi, C.; Meneghesso, G.; Zanoni, E.; Meneghini, M. Review and Outlook on GaN and SiC Power Devices: Industrial State-of-the-Art, Applications, and Perspectives. *IEEE Transactions on Electron Devices* **2024**, *71*, 1344–1355. <https://doi.org/10.1109/TED.2023.3346369>.
9. Vitale, G. Energy Saving by Power Electronics: Towards a New Concept of Renewable Source. *Renewable Energy and Power Quality Journal* **2016**, *4*, 160001–160010. <https://doi.org/10.24084/repqj14.001>.
10. Infineon Technologies AG. Scaling AI Data Center Power Delivery with Si, SiC, and GaN: Power Supply Units from 3 to 12 kW. Technical report, Infineon Technologies, 2024.
11. IDTechEx Research. Power Electronics for Electric Vehicles 2025-2035: Technologies, Markets, and Forecasts. Technical report, IDTechEx, 2024.
12. STMicroelectronics. Fourth Generation STPOWER Silicon Carbide (SiC) MOSFET Technology for Next-Generation EV Traction Inverters. Technical report, STMicroelectronics, 2024.
13. Page, M.J.; McKenzie, J.E.; Bossuyt, P.M.; Boutron, I.; Hoffmann, T.C.; Mulrow, C.D.; Shamseer, L.; Tetzlaff, J.M.; Akl, E.A.; Brennan, S.E.; et al. The PRISMA 2020 Statement: An Updated Guideline for Reporting Systematic Reviews. *BMJ* **2021**, *372*, n71. <https://doi.org/10.1136/bmj.n71>.
14. Rafin, S.S.H.; Ahmed, R.; et al. Power Electronics Revolutionized: A Comprehensive Analysis of Emerging Wide and Ultrawide Bandgap Devices. *Micromachines* **2023**, *14*, 2045. <https://doi.org/10.3390/mi14112045>.
15. Chow, T.P.; et al. Wide-Bandgap Semiconductors and Power Electronics as Pathways to Carbon Neutrality. *Nature Reviews Electrical Engineering* **2025**, *2*, 1–15. <https://doi.org/10.1038/s44287-024-00135-5>.
16. Kumar, A.; Moradpour, M.; Losito, M.; Franke, W.T.; Ramasamy, S.; Baccoli, R.; Gatto, G. Wide Band Gap Devices and Their Application in Power Electronics. *Energies* **2022**, *15*. <https://doi.org/10.3390/en15239172>.
17. She, X.; Huang, A.Q.; Lucía, O.; Ozpineci, B. Review of Silicon Carbide Power Devices and Their Applications. *IEEE Transactions on Industrial Electronics* **2017**, *64*, 8193–8205. <https://doi.org/10.1109/TIE.2017.2652401>.
18. Musumeci, S.; Barba, V. Gallium Nitride Power Devices in Power Electronics Applications: State of Art and Perspectives. *Energies* **2023**, *16*. <https://doi.org/10.3390/en16093894>.
19. Belguith, M.; Eloued, S.; Kadi, M.; Ben Hadj Slama, J.; Hamouda, M. A Review of Thermal Management Techniques Adopted for High-Power-Density GaN-Based Converters. *Chips* **2026**, *5*. <https://doi.org/10.3390/chips5010004>.
20. Qin, Y.; Albano, B.; Spencer, J.; Lundh, J.S.; Wang, B.; Buttay, C.; Tadjer, M.; DiMarino, C.; Zhang, Y. Thermal management and packaging of wide and ultra-wide bandgap power devices: a review and perspective. *Journal of Physics D: Applied Physics* **2023**, *56*, 093001. <https://doi.org/10.1088/1361-6463/acb4ff>.
21. Zhou, J.; Zhong, L.; Feng, X.; Zhang, W.; Liu, X.; Zhou, H.; Liu, Z.; Hao, Y.; Zhang, J. Recent Advances in Device-Level Thermal Management Technologies for Wide Bandgap Semiconductor: A Review. *IEEE Transactions on Electron Devices* **2025**, *72*, 2769–2782. <https://doi.org/10.1109/ted.2025.3562506>.
22. Zhang, B.; Wang, S. A Survey of EMI Research in Power Electronics Systems With Wide-Bandgap Semiconductor Devices. *IEEE Journal of Emerging and Selected Topics in Power Electronics* **2020**, *8*, 626–643. <https://doi.org/10.1109/JESTPE.2019.2953730>.
23. Donato, N.; Rouger, N.; Pernot, J.; Longobardi, G.; Udrea, F. Diamond power devices: state of the art, modelling, figures of merit and future perspective. *Journal of Physics D: Applied Physics* **2019**, *53*, 093001. <https://doi.org/10.1088/1361-6463/ab4eab>.
24. Green, A.J.; Speck, J.; Xing, G.; Moens, P.; Allerstam, F.; Gumaelius, K.; Neyer, T.; Arias-Purdue, A.; Mehrotra, V.; Kuramata, A.; et al. β -Gallium oxide power electronics. *APL Materials* **2022**, *10*, 029201. <https://doi.org/10.1063/5.0060327>.

25. Akbar, G.; Di Fatta, A.; Rizzo, G.; Ala, G.; Romano, P.; Imburgia, A. Comprehensive Review of Wide-Bandgap (WBG) Devices: SiC MOSFET and Its Failure Modes Affecting Reliability. *Physchem* **2025**, *5*. <https://doi.org/10.3390/physchem5010010>.
26. Adeloye, I.A.; Bhattacharya, I.; Ezugwu, E.O.; Antony Dhasan, M.V. GaN Electric Vehicle Systems—A Comparative Review. *Energies* **2025**, *18*. <https://doi.org/10.3390/en18226020>.
27. Wu, X.; Zhang, L.; You, H.; Zhang, S.; Nikolov, D.; Cui, Q. EMC-Friendly Gate Driver Design in GaN-Based DC-DC Converters for Automotive Electronics: A Review. *Electronics* **2026**, *15*, 283. <https://doi.org/10.3390/electronics15020283>.
28. Ambacher, O.; et al. Two-Dimensional Electron Gases Induced by Spontaneous and Piezoelectric Polarization Charges. *Journal of Applied Physics* **1999**, *85*, 3222–3233. <https://doi.org/10.1063/1.369664>.
29. Razeeb, K.M.; et al. Present and Future Thermal Interface Materials for Electronic Devices. *International Materials Reviews* **2018**, *63*, 1–21. <https://doi.org/10.1080/09506608.2017.1296605>.
30. Baliga, B.J. Power Semiconductor Device Figure of Merit for High-Frequency Applications. *IEEE Electron Device Letters* **1989**, *10*, 455–457. <https://doi.org/10.1109/55.43098>.
31. Johnson, E.O. Physical Limitations on Frequency and Power Parameters of Transistors. *RCA Review* **1965**, *26*, 163–177. https://doi.org/10.1142/9789814503464_0032.
32. Keyes, R.W. Figure of Merit for Semiconductors for High-Speed Switches. *Proceedings of the IEEE* **1972**, *60*, 225. <https://doi.org/10.1109/PROC.1972.8593>.
33. Hudgins, J.L.; Simin, G.S.; Santi, E.; Khan, M.A. An Assessment of Wide Bandgap Semiconductors for Power Devices. *IEEE Transactions on Power Electronics* **2003**, *18*, 907–914. <https://doi.org/10.1109/TPEL.2003.810840>.
34. Baliga, B. Trends in power semiconductor devices. *IEEE Transactions on Electron Devices* **1996**, *43*, 1717–1731. <https://doi.org/10.1109/16.536818>.
35. Qin, Y.; Wang, Z.; Sasaki, K.; Ye, J.; Zhang, Y. Recent progress of Ga₂O₃ power technology: large-area devices, packaging and applications. *Japanese Journal of Applied Physics* **2023**, *62*, SF0801. <https://doi.org/10.35848/1347-4065/acb3d3>.
36. Herath Mudiyanse, D.; Da, B.; Adivarahan, J.; Wang, D.; He, Z.; Fu, K.; Zhao, Y.; Fu, H. β -Ga₂O₃-Based Heterostructures and Heterojunctions for Power Electronics: A Review of the Recent Advances. *Electronics* **2024**, *13*. <https://doi.org/10.3390/electronics13071234>.
37. Wang, L.; Cheng, J.; Qu, K.; Zhu, Q.; Tian, B.; Yang, Z. Aluminum-Nitride-Based Semiconductors: Growth Processes, Ferroelectric Properties, and Performance Enhancements. *Inorganics* **2025**, *13*. <https://doi.org/10.3390/inorganics13020029>.
38. Haque, A.; Taqy, S.; Narayan, J. Recent Progress in Cubic Boron Nitride (c-BN) Fabrication by Pulsed Laser Annealing for Optoelectronic Applications. *Journal of Electronic Materials* **2024**, *53*, 4308–4340. <https://doi.org/10.1007/s11664-024-11171-0>.
39. Zhang, X. Doping and electrical properties of cubic boron nitride thin films: A critical review. *Thin Solid Films* **2013**, *544*, 2–12. The 6th International Conference on Technological Advances of Thin Films & Surface Coatings, <https://doi.org/10.1016/j.tsf.2013.07.001>.
40. Haque, A.; Narayan, J. Tunable n-Type Conductivity and Transport Properties of Cubic Boron Nitride via Carbon Doping. *ACS Applied Electronic Materials* **2021**, *3*, 1359–1367, [<https://doi.org/10.1021/acsaelm.0c01130>]. <https://doi.org/10.1021/acsaelm.0c01130>.
41. Narayan, J.; Bhaumik, A. Direct Conversion of h-BN into c-BN and Formation of Epitaxial c-BN/Diamond Heterostructures. *Journal of Applied Physics* **2016**, *119*, 185302. <https://doi.org/10.1063/1.4948688>.
42. Mullen, J.T.; et al. Electronic Properties of c-BN/Diamond Heterostructures for High-Frequency High-Power Applications. *Diamond and Related Materials* **2024**, *143*, 110920. <https://doi.org/10.1016/j.diamond.2024.110920>.
43. Jones, E.A.; Wang, F.F.; Costinett, D. Review of Commercial GaN Power Devices and GaN-Based Converter Design Challenges. *IEEE Journal of Emerging and Selected Topics in Power Electronics* **2016**, *4*, 707–719. <https://doi.org/10.1109/JESTPE.2016.2582685>.
44. Lidow, A.; Strydom, J.; de Rooij, M.; Reusch, D. *GaN Transistors for Efficient Power Conversion*; John Wiley & Sons: Hoboken, NJ, USA, 2014. <https://doi.org/10.1002/9781118844779>.
45. Kimoto, T.; Cooper, J.A. *Fundamentals of Silicon Carbide Technology*; Wiley-IEEE Press: Hoboken, NJ, USA, 2014. <https://doi.org/10.1002/9781118313534>.
46. Nakamura, T.; et al. High Performance SiC Trench Devices with Ultra-Low Ron. In Proceedings of the Proceedings of the IEEE International Electron Devices Meeting (IEDM), 2011, pp. 26.5.1–26.5.3. <https://doi.org/10.1109/IEDM.2011.6131619>.

47. Chen, K.J.; et al. GaN-on-Si Power Technology: Devices and Applications. *IEEE Transactions on Electron Devices* **2017**, *64*, 779–795. <https://doi.org/10.1109/TED.2017.2657579>.
48. Huang, X.; Li, Q.; Liu, Z.; Lee, F.C. Analytical loss model of high voltage GaN HEMT in cascode configuration. In Proceedings of the 2013 IEEE Energy Conversion Congress and Exposition, 2013, pp. 3587–3594. <https://doi.org/10.1109/ECCE.2013.6647173>.
49. Uemoto, Y.; et al. Gate Injection Transistor (GIT)—A Normally-Off AlGaN/GaN Power Transistor. *IEEE Transactions on Electron Devices* **2007**, *54*, 3393–3399. <https://doi.org/10.1109/TED.2007.908601>.
50. Meneghini, M.; Modolo, N.; Nardo, A.; De Santi, C.; Minetto, A.; Sayadi, L.; Koller, C.; Sicre, S.; Prechtel, G.; Meneghesso, G.; et al. Charge Trapping in GaN Power Transistors: Challenges and Perspectives. In Proceedings of the 2021 IEEE BiCMOS and Compound Semiconductor Integrated Circuits and Technology Symposium (BCICTS), 2021, pp. 1–4. <https://doi.org/10.1109/BCICTS50416.2021.9682455>.
51. Shenoy, P.M.; et al. Vertical GaN MOSFET Power Devices. *Micromachines* **2023**, *14*, 1937. <https://doi.org/10.3390/mi14101937>.
52. Liu, J.; Xiao, M.; Zhang, R.; Pidaparathi, S.; Cui, H.; Edwards, A.; Craven, M.; Baubutr, L.; Drowley, C.; Zhang, Y. 1.2-kV Vertical GaN Fin-JFETs: High-Temperature Characteristics and Avalanche Capability. *IEEE Transactions on Electron Devices* **2021**, *68*, 2025–2032. <https://doi.org/10.1109/TED.2021.3059192>.
53. You, S.; Geens, K.; Borga, M.; Liang, H.; Hahn, H.; Fahle, D.; Heuken, M.; Mukherjee, K.; Santi, C.D.; Meneghini, M.; et al. Vertical GaN devices: Process and reliability. *Microelectronics Reliability* **2021**, *126*, 114218. <https://doi.org/https://doi.org/10.1016/j.microrel.2021.114218>.
54. Biela, J.; Schweizer, M.; Waffler, S.; Kolar, J.W. SiC versus Si—Evaluation of Potentials for Performance Improvement of Inverter and DC–DC Converter Systems by SiC Power Semiconductors. *IEEE Transactions on Industrial Electronics* **2011**, *58*, 2872–2882. <https://doi.org/10.1109/TIE.2010.2072896>.
55. Su, H.; Zhang, L.; Meng, D.; Li, Y.; Han, N.; Xia, Y. Modeling and Evaluation of SiC Inverters for EV Applications. *Energies* **2022**, *15*. <https://doi.org/10.3390/en15197025>.
56. Whitaker, B.; et al. A High-Density, High-Efficiency, Isolated On-Board Vehicle Battery Charger Utilizing SiC Power Devices. *IEEE Transactions on Power Electronics* **2014**, *29*, 2606–2617. <https://doi.org/10.1109/TPEL.2013.2279950>.
57. Pudur, R.; Rajak, M.K. A comprehensive review of grid-connected inverter topologies and control strategies (2020–2025). *Next Energy* **2025**, *9*, 100433. <https://doi.org/https://doi.org/10.1016/j.nxener.2025.100433>.
58. Reusch, D.; Strydom, J. Understanding the Effect of PCB Layout on Circuit Performance in a High-Frequency Gallium-Nitride-Based Point of Load Converter. *IEEE Transactions on Power Electronics* **2014**, *29*, 2008–2015. <https://doi.org/10.1109/TPEL.2013.2266103>.
59. Cohen, L.; Bernstein, J.B.; Aharon, I. Gate Driver for High-Frequency Power Converter. *Electronics* **2025**, *14*. <https://doi.org/10.3390/electronics14020224>.
60. Erickson, R.W.; Maksimović, D. *Fundamentals of Power Electronics*, 2nd ed.; Springer: Boston, MA, USA, 2001. <https://doi.org/10.1007/b100747>.
61. Renuka Varma, P.C.; Kshirsagar, A. Soft Switched Interleaved Buck Converter for High Power Applications. In Proceedings of the 2025 IEEE Energy Conversion Congress & Exposition Asia (ECCE-Asia), 2025, pp. 1–5. <https://doi.org/10.1109/ECCE-Asia63110.2025.11112000>.
62. De Doncker, R.; Divan, D.; Kheraluwala, M. A three-phase soft-switched high-power-density DC/DC converter for high-power applications. *IEEE Transactions on Industry Applications* **1991**, *27*, 63–73. <https://doi.org/10.1109/28.67533>.
63. Kheraluwala, M.H.; Gascoigne, R.W.; Divan, D.M.; Baumann, E.D. Performance Characterization of a High-Power Dual Active Bridge DC-DC Converter. *IEEE Transactions on Industry Applications* **1992**, *28*, 1294–1301. <https://doi.org/10.1109/28.175280>.
64. Hurley, W.G.; Wölfle, W.H. *Transformers and Inductors for Power Electronics*; Wiley: Chichester, UK, 2013. <https://doi.org/10.1002/9781118544648>.
65. Everts, J. Design and Optimization of an Efficient (96.1kW/dm³) Bidirectional Isolated Single-Phase Dual Active Bridge AC-DC Converter. *Energies* **2016**, *9*. <https://doi.org/10.3390/en9100799>.
66. Badawi, N.; Hilt, O.; Behat-Treidel, E.; Böcker, J.; Würfl, J.; Dieckerhoff, S. Investigation of the dynamic on-state resistance of 600V normally-off and normally-on GaN HEMTs. In Proceedings of the 2015 IEEE Energy Conversion Congress and Exposition (ECCE), 2015, pp. 913–919. <https://doi.org/10.1109/ECCE.2015.7309785>.

67. Han, D.; Li, S.; Wu, Y.; Choi, W.; Sarlioglu, B. Comparative Analysis on Conducted CM EMI Emission of Motor Drives: WBG Versus Si Devices. *IEEE Transactions on Industrial Electronics* **2017**, *64*, 8353–8363. <https://doi.org/10.1109/TIE.2017.2681968>.
68. Zahwan, N.S.H.M.; Hasan, K.N.M.; Bin Zakaria, Z.A. Performance Analysis of SiC and GaN-Based Traction Inverter in Electric Vehicle Drive System. In Proceedings of the 2024 IEEE Sustainable Power and Energy Conference (iSPEC), 2024, pp. 681–686. <https://doi.org/10.1109/iSPEC59716.2024.10892532>.
69. Wang, J.; Xu, Z.; Wang, X.; Zhao, Y.; Liu, G.; Tian, R.; Jing, L. Design of Integrated Magnetic Transformer for High Frequency LLC Converter. In Proceedings of the 2020 4th International Conference on HVDC (HVDC), 2020, pp. 986–991. <https://doi.org/10.1109/HVDC50696.2020.9292690>.
70. Musavi, F.; Eberle, W. Overview of Wireless Power Transfer Technologies for Electric Vehicle Battery Charging. *IET Power Electronics* **2014**, *7*, 60–66. <https://doi.org/10.1049/iet-pel.2013.0047>.
71. Lee, H.; Smet, V.; Tummala, R. A Review of SiC Power Module Packaging Technologies: Challenges, Advances, and Emerging Issues. *IEEE Journal of Emerging and Selected Topics in Power Electronics* **2020**, *8*, 239–255. <https://doi.org/10.1109/JESTPE.2019.2951801>.
72. Er, B.; Bavtar, G.; Kivanc, O.C. Design and Implementation of a High Power Density GaN-Based USB-PD Charger. In Proceedings of the 2025 IEEE 19th International Conference on Compatibility, Power Electronics and Power Engineering (CPE-POWERENG), 2025, pp. 1–5. <https://doi.org/10.1109/CPE-POWERENG63314.2025.11027249>.
73. Ciappa, M. Selected Failure Mechanisms of Modern Power Modules. *Microelectronics Reliability* **2002**, *42*, 653–667. [https://doi.org/10.1016/S0026-2714\(02\)00042-2](https://doi.org/10.1016/S0026-2714(02)00042-2).
74. Wang, H.; Blaabjerg, F. Reliability of Capacitors for DC-Link Applications in Power Electronic Converters—An Overview. *IEEE Transactions on Industry Applications* **2014**, *50*, 3569–3578. <https://doi.org/10.1109/TIA.2014.2308357>.
75. Lelis, A.J.; Green, R.; Habersat, D.B.; El, M. Basic Mechanisms of Threshold-Voltage Instability and Implications for Reliability Testing of SiC MOSFETs. *IEEE Transactions on Electron Devices* **2015**, *62*, 316–323. <https://doi.org/10.1109/TED.2014.2356172>.
76. Zhu, H.; Matioli, E. Accurate Measurement of Dynamic ON-Resistance in GaN Transistors at Steady-State. *IEEE Transactions on Power Electronics* **2023**, *38*, 8045–8050. <https://doi.org/10.1109/TPEL.2023.3268890>.
77. Jin, D.; del Alamo, J.A. Mechanisms responsible for dynamic ON-resistance in GaN high-voltage HEMTs. In Proceedings of the 2012 24th International Symposium on Power Semiconductor Devices and ICs, 2012, pp. 333–336. <https://doi.org/10.1109/ISPSD.2012.6229089>.
78. Qiu, X.; Zhang, X.; Lu, P.; Wei, S. Research on Low-Inductance Packaging Design and Switching Characteristics of GaN HEMT Half-Bridge Modules for High-Frequency Converters. In Proceedings of the 2025 International Conference on Advanced Energy Systems and Power Electronics (AESPE), 2025, pp. 29–33. <https://doi.org/10.1109/AESPE65805.2025.11162803>.

Disclaimer/Publisher’s Note: The statements, opinions and data contained in all publications are solely those of the individual author(s) and contributor(s) and not of MDPI and/or the editor(s). MDPI and/or the editor(s) disclaim responsibility for any injury to people or property resulting from any ideas, methods, instructions or products referred to in the content.